Science of the Total Environment 672 (2019) 1004–1016

Contents lists available at ScienceDirect

Science of the Total Environment

journal homepage: www.elsevier.com/locate/scitotenv

Distribution of ^{137}Cs in the Bohai Sea, Yellow Sea and East China Sea: Sources, budgets and environmental implications

Fule Zhang, Jinlong Wang *, Dantong Liu, Qianqian Bi, Jinzhou Du

State Key Laboratory of Estuarine and Coastal Research, East China Normal University, Shanghai 200241, China

HIGHLIGHTS

- The spatial distribution of ^{137}Cs in surface sediments and seawater was investigated.
- Oceanic inputs dominate the source of ^{137}Cs in eastern Chinese seas.
- The apparent half-lives of ^{137}Cs are 7.7–15.1 y in eastern Chinese seas.
- ^{137}Cs is useful to track fine sediment transport in river-dominated marginal seas.
- ^{137}Cs is useful to trace water mass movement and exchange in marginal seas.

GRAPHICAL ABSTRACT

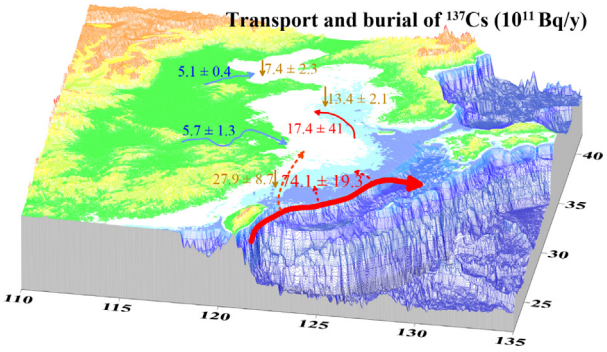

ARTICLE INFO

Article history:
Received 6 January 2019
Received in revised form 28 March 2019
Accepted 1 April 2019
Available online 2 April 2019

Editor: Mae Sexauer Gustin

Keywords:
^{137}Cs
Water mass
Sediment transport
Marginal seas
Mass balance

ABSTRACT

The transport processes and fate of ^{137}Cs in eastern Chinese seas (ECSs) that consists of the Bohai, Yellow, and East China Seas, have not been well established. In this study, we measured the concentrations of ^{137}Cs in the ECSs water and surface sediments during 2013–2014. Combined with a number of published ^{137}Cs inventory data from drainage basins and sediment accumulation rates in the ECSs, the distribution, sources and budgets of ^{137}Cs in the ECSs were investigated. The ^{137}Cs activity in the water column and surface sediments ranged from 0.03 to 1.92 Bq/m^3 and from 0.30 to 5.22 Bq/kg, respectively. No ^{134}Cs signal was observed, suggesting that the Fukushima accident had limited impact on the ECSs during the investigation period. Mass balance of ^{137}Cs suggests that at least 7.4×10^{12} Bq/y of ^{137}Cs imported into the ECSs from the Northwestern Pacific that accounts for 0.7% of the ^{137}Cs transported by the Kuroshio Current, and this value is 5.2 times higher than the sum of atmospheric fallout and total riverine input. The apparent half-lives of ^{137}Cs are estimated to be 15.1 y for the ECS and 7.7 y for the YS. The vertical profiles in the continental shelf edge and the Yangtze River Estuary reveal that the upwelling of the Kuroshio Subsurface Water is the main mechanism of ^{137}Cs import into the ECSs. The high level of ^{137}Cs in oceanic water masses and the low level of ^{137}Cs in riverine and coastal waters make ^{137}Cs a good indicator for tracing water mass movement and interaction. In addition, good correlation between ^{137}Cs activity and mean grain size (φ) indicates that ^{137}Cs can serve as an effective tracer to track dispersal pathways of fine sediments in river-dominated marginal seas.

* Corresponding author.
E-mail address: jlwang@sklec.ecnu.edu.cn (J. Wang).

https://doi.org/10.1016/j.scitotenv.2019.04.001
0048-9697/

1. Introduction

Anthropogenic radionuclides have been introduced to marine environments by atmospheric deposition as a consequence of atmospheric nuclear weapons testing, nuclear accidents, and discharges from nuclear installations. Among these radionuclides, ^{137}Cs has received the most attention not only due to its long half-life (30.17 years) and high radiotoxicity, but also for its implication as a powerful tool for oceanography. Considering the well-defined origin and conservative behavior of ^{137}Cs in the open ocean, it is useful to trace water mass movement, mixing, and circulation (Bowen et al., 1980; Aarkrog et al., 1983; Cochran et al., 1987; Aoyama et al., 2011). Moreover, vertical distribution of ^{137}Cs in sediment cores is widely utilized for reconstruction of sedimentary deposition history (Fuller et al., 1999; Su and Huh, 2002; Pfitzner et al., 2004; Wang et al., 2016).

The Pacific Ocean is recognized as a major recipient of ^{137}Cs not only because of its sheer size, but also due to the presence of the North Pacific Proving Grounds (NPPG) in the Marshall Islands (Povinec et al., 2004). ^{137}Cs in the Pacific Ocean has two major sources: global fallout and close-in fallout from the NPPG (Bowen et al., 1980; Yamada et al., 2006). Aarkrog (2003) has estimated that the ^{137}Cs from global fallout to the Pacific was approximately 311 PBq, while the close-in fallout of ^{137}Cs from the NPPG may be on the order of 100 PBq. In addition, the deposition rates of ^{137}Cs from global fallout varied by latitude, and the highest deposition occurred in the mid-latitudes of the Northwestern Pacific (WNP) (Aoyama et al., 2006). More recently, the Fukushima accident caused a large amount of ^{137}Cs to be released, and most estimates suggested that the ^{137}Cs released into the WNP ranged from 15 PBq to 20 PBq (Tsubono et al., 2016; Aoyama et al., 2016; Buesseler et al., 2017). Therefore, the Pacific Ocean, especially the WNP, has always been a hotspot of ^{137}Cs study. The distribution, transport processes and fate of ^{137}Cs in the WNP have already been intensively investigated in a series of studies (e.g. Bowen et al., 1980; Aoyama and Hirose, 1995; Povinec et al., 2003; Yamada et al., 2006), but have not been well discussed in its marginal seas—the eastern Chinese seas (ECSs) that include the Bohai Sea (BS), Yellow Sea (YS) and East China Sea (ECS), only some outdated and low resolution data have been reported (Nagaya and Nakamura, 1992; Wu et al., 2013). The ECSs link the world's largest continent (Asia–Europe) and ocean (Pacific Ocean). Considering the conservative feature of ^{137}Cs in seawater, it can be entrained in the northward flowing Kuroshio Current (KC), a branch of the North Equatorial Current (NEC), and then spread widely to the WNP and its marginal seas. This long-range transport process has been confirmed by $^{239+240}$Pu and their atom ratios (Yamada et al., 2006; Liu et al., 2011; Wang et al., 2017a). By comparing concentrations of ^{137}Cs in the coastal seawater of Japan, Kasamatsu and Inatomi (1998) pointed out that surface water with a higher ^{137}Cs concentration is transported from the WNP via the Tsushima Current (TC), a branch of the KC. The similar ^{137}Cs activities in the Japan/East Sea and WNP also suggested that ^{137}Cs from the NPPG can be transported to the Japan/East Sea (Ito et al., 2003; Povinec et al., 2004). The ECSs are located between the Japan/East sea and the WNP; thus, it is reasonable to believe that ^{137}Cs from the WNP can be transported into the ECSs. However, a study of the behavior and fate of ^{137}Cs in the ECSs is still limited.

The ECSs are typical river-dominated marginal seas. The Yangtze River and Yellow River, the two largest rivers on the Eurasian continent, discharge ~1.6 billion tons of sediments annually to the ECSs, accounting for 10% of the world's annual sediment discharge (Milliman and Farnsworth, 2013). These sediments can carry many terrestrial particles that can bond with ^{137}Cs, which could affect the distribution and inventory of the ^{137}Cs in the ECSs. Most importantly, the enormous riverine sediment discharge leads to a high concentration of suspended particles in the ECSs. Meanwhile, the current system in the ECSs is complex and the water depth is shallow, and therefore, the behavior of the ^{137}Cs in the ECSs is believed to be quite different from the open ocean. In general, the scavenging and burying processes by association with the particles could be more intensive than those in the open ocean (Carpenter et al., 1987; Nagaya and Nakamura, 1992). In addition, boundary scavenging processes could occur in the highly turbid water column of the nearshore areas and enhance the import of ^{137}Cs from offshore areas (Du et al., 2010). These characteristics make the transport processes of ^{137}Cs in the ECSs complicated.

In our previous work, the results showed that oceanic input is a dominant source of ^{137}Cs in the ECS (Du et al., 2010; Zhao et al., 2018). Now we extend our research to the ECSs and present more comprehensive data to do the following: (i) describe the distribution characteristics of ^{137}Cs in the water column and surface sediments in the ECSs; (ii) construct the ^{137}Cs budget in the ECSs within a source-sink perspective by calculating the atmospheric fallout, riverine input, oceanic input, natural decay, and burial flux; (iii) evaluate the tracer application of ^{137}Cs in marine environments. We quantify the interlinked budget balance of ^{137}Cs between the BS, YS and ECS. This work will contribute to our understanding of not only the transport processes and ultimate fate of ^{137}Cs but also the biogeochemical cycles of other analog materials in river-dominated marginal seas.

2. Materials and methods

2.1. Study area

The ECSs are surrounded by mainland China, the Korean Peninsula, Taiwan Island and Ryukyu Island. There are many rivers flowing into the ECSs including the Yangtze River and Yellow River, two of the largest river systems in the world (Fig. 1). The BS is a Chinese inland sea with an average water depth of 18 m, connected with the YS by the Bohai Strait. The YS is a typical semienclosed epicontinental sea between the BS and ECS, with an average water depth of 44 m. The YS is separated from the ECS to the south by an arbitrary line connecting the north of the Yangtze River mouth with Cheju Island. The ECS is a very broad and flat continental shelf sea, with a maximum width of 640 km. Based on the water depth, it can be divided into an inner-shelf area, outer-shelf area and slope, and Okinawa Trough area, with water depths below 70 m, between 70 m and 200 m and above 200 m, respectively (Su and Huh, 2002). The ECS, together with the YS and BS, constitute a series of interlinked marginal seas in the WNP.

Due to effect of monsoon, Kuroshio Current, fluvial runoff and tidal motion, the circulation pattern in the ECSs is very complex and dynamic (Fig. 1), as described in Su (2001). In general, there are two current systems of which one is warm and salty current system of oceanic origin, and another one is cold and diluted coastal current system (Guan, 1994). The former moves northward including the Kuroshio Current (KC) along the edge of the ECS continental shelf and the Taiwan Warm Current (TWC) from the Taiwan Strait. The Yellow Sea Warm Current (YSWC) is a branch of KC and flows northwest into the YS, and its extension can reach the BS through northern Bohai Strait. As for coastal current system, most of coastal currents flow southward including the Bohai Sea Coastal Current (BSCC), Yellow Sea Costal Current (YSCC) and West Korea Coastal Current (WKCC), while the Zhejiang-Fujian Coastal Current (ZFCC) flows northward in summer and southward in winter owing to the change of prevailing monsoon. The Changjiang Diluted Water (CDW) flows toward northeast in flood season and turns to south in dry season.

2.2. Sampling and analysis

Two cruises onboard the R/V "Dongfanghong 2" were conducted in the ECS during 6 to 28 August 2013 and in the YS-BS during 28 April to 17 May 2014. A total of 107 seawater samples (including 83 surface samples and 24 deep layer samples) and 148 surface sediment samples (0–1 cm) were collected (Fig. 1). Surface seawater samples (0–0.5 m) were collected by a submersible pump and deep layer samples were collected by using a CTD rosette system. All water samples filtered

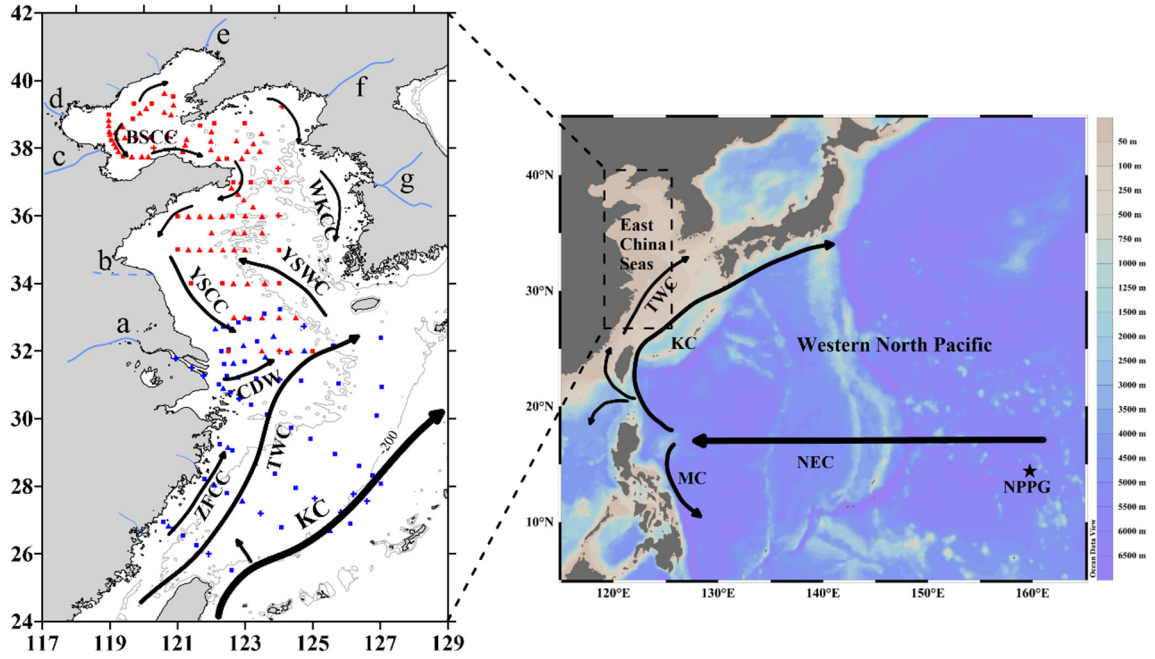

Fig. 1. Map showing the sampling locations and circulation pattern in the Eastern Chinese Seas. Sampling stations in August 2013 and May 2014 are marked in blue color and red color, respectively. Triangle symbols represent that only surface sediments were collected at that station. Cross symbols represent only seawater samples were collected. Square symbols represent both sediment and seawater samples were collected. Regional ocean circulation pattern is modified from Su (2001) and Hu et al. (2015). BSCC: Bohai Sea Coastal Current; YSCC: Yellow Sea Costal Current; YSWC: Yellow Sea Warm Current; WKCC: West Korea Coastal Current; CDW: Changjiang Diluted Water; ZFCC: Zhejiang-Fujian Coastal water; TWC: Taiwan Warm Current; KC: Kuroshio Current; NEC: North Equatorial Current; MC: Mindanao Current. Several large rivers are also plotted, including a: Yangtze River, b: old Yellow River, c: Yellow River, d: Haihe, e: Liaohe, f: Yalujiang, g: Han River.

through a pre-cleaned special polypropylene cartridge with 0.5 μm pore-size (Wang et al., 2017b). Sediment samples were collected using a box sampler, then placed in polyethylene bags and frozen in a refrigerator for further analysis.

^{137}Cs activities in seawater samples were measured following the method described by Zhao et al. (2018). Briefly, filtered seawater samples (~100 L each) were acidified to pH < 2 with concentrated HCl, then added 25 mg CsCl as carrier and chemical yield tracer. After equilibration, 40 g ammonium phosphomolybdate (AMP) was added and stirred for 30 min until well mixed. After settling about 24 h, the supernatants were siphoned out, then the residual was transferred into a 2 L plastic bottle and brought back to the laboratory. In lab, the residual was centrifuged and freeze-dried for three days to separate AMP-Cs precipitate. The dried sample was homogenized and sealed in a plastic tube. Finally, the activities of ^{137}Cs in prepared samples were measured using a well-type HPGe gamma spectrometer (GWL-120210-S, ORTEC). ^{137}Cs was detected at 661.6 keV peak with the branch ratio of 85.1%. In addition, considering the Fukushima accident, ^{134}Cs was also concerned during the measurement, however, there was no signal at 604 keV in gamma spectrums. The mean chemical recovery was 77.8% ± 3.2%, obtained by using the atomic absorption spectrophotometer (AA-800, Perkin-Elmer) to determine stable Cs in the AMP-Cs precipitate. The IAEA standard source (IAEA-447) was analyzed for quality control, and the result agreed with the certificated value well.

The sediment samples were oven dried at 60 °C for several days. An aliquot of dry sediments was used to determine the grain size. Briefly, 0.1–0.2 g sediments were placed in beakers, then added 5 mL 10% H_2O_2 and 5 mL 0.2 M HCl to remove organic matter and coatings of metal oxides. After about 24 h, 10 mL 0.5 M sodium hexametaphosphate solution was added and oscillated in ultrasonic bath for 10 min to make the sediments disaggregate completely, then analyzed by using a laser particle analyzer (LS100Q, Beckman, USA). Determination of ^{137}Cs activities in sediments followed the method described by Du et al. (2010). The dried sample was ground, homogenized, and sealed in a plastic box (70 mm diameter × 70 mm height), then measured by a HPGe γ-ray detector (ADC-1000-I, ORTEC) with a relative counting efficiency of 35% and an energy resolution of 1.8 keV (at 1332 keV). Data reported for ^{137}Cs in all samples were decay-corrected to sampling date.

3. Results

3.1. Spatial distribution of ^{137}Cs in ECSs' surface water

The temperature, salinity and ^{137}Cs activity in the ECSs' waters are listed in the Supplemental file (Table S1). The spatial distribution of ^{137}Cs activity in the surface waters of the ECSs are shown in Fig. 2. In the ECS, ^{137}Cs activity ranged between 0.12 and 1.59 Bq/m^3 (mean: 0.62 ± 0.32 Bq/m^3, n = 53). The highest ^{137}Cs concentration was observed in the shelf edge area of the ECS, while the lowest was found in the Yangtze Estuary and extended to the northeast to Cheju island (Fig. 2a). Our results were lower than the values observed in the Northwest Pacific (1.0–2.2 Bq/m^3, mean: 1.6 ± 0.4 Bq/m^3, decay-corrected to 2014) (Povinec et al., 2003), East China Sea (0.70–1.33 Bq/m^3, mean: 1.05 ± 0.07 Bq/m^3, decay-corrected to 2014) (Wu et al., 2013), South China Sea (0.99–1.41 Bq/m^3, mean: 1.12 ± 0.14 Bq/m^3) (Wu, 2018) and Luzon Strait (0.43–2.44 Bq/m^3, mean: 1.04 ± 0.13 Bq/m^3) (Zhou et al., 2018). ^{137}Cs concentrations in the surface waters of the YS and BS were generally low, ranging 0.08–0.68 Bq/m^3 (mean: 0.38 ± 0.17 Bq/m^3, n = 21) and 0.03–0.09 Bq/m^3 (mean: 0.05 ± 0.02 Bq/m^3, n = 9), respectively (Fig. 2b). The southern region of the YS had higher ^{137}Cs activities, with a sharply decreasing trend northward, but smoothly westward. The ^{137}Cs activities in the YS were much lower than results measured in 1987 (2.93–4.56 Bq/m^3, mean:3.80 ± 0.70 Bq/m^3) (Nagaya and Nakamura, 1992) and in 1999–2000 (1.62–3.41 Bq/m^3, mean:2.7 ± 0.2 Bq/m^3) (Hong et al., 2006), showing a decreasing trend over time.

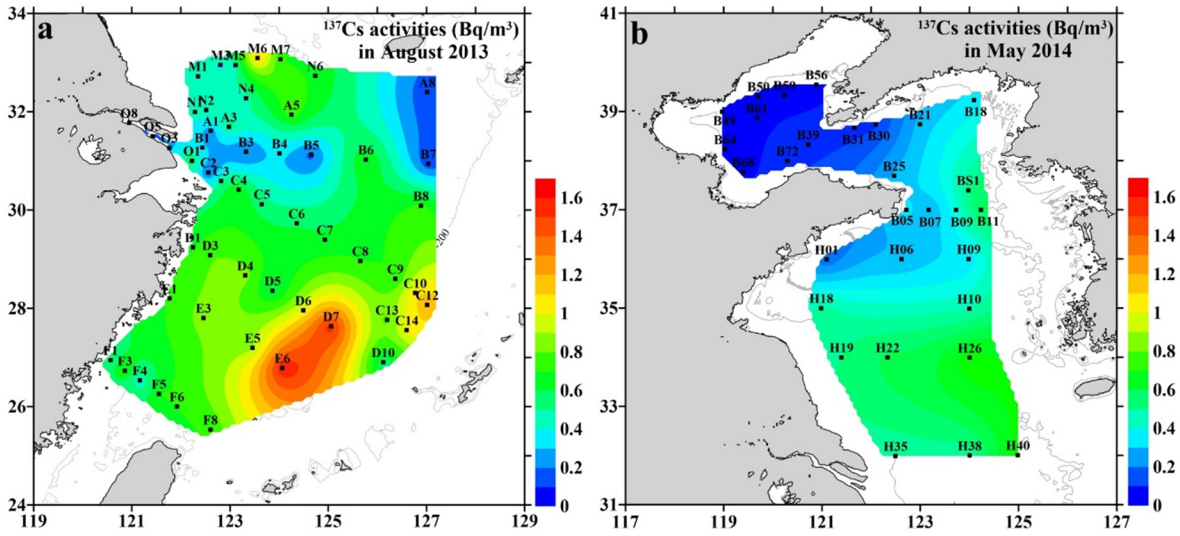

Fig. 2. Spatial distribution of ^{137}Cs activities in the surface water of the ECS (a) and YS-BS (b).

3.2. Vertical profiles of ^{137}Cs in the water column

Fig. 3 shows the vertical profiles of ^{137}Cs activities in the ECSs. At a few stations on the ECS shelf edge (e.g., F8, D10, C12 and C13), ^{137}Cs activity maxima were observed in the subsurface layer at a depth of 100–200 m (Fig. 3a), although the sampling depth did not cover the entire water column. In fact, similar ^{137}Cs profiles have been observed in the subtropical and equatorial North Pacific, with ^{137}Cs peaking at approximately 200 m depth (Aoyama et al., 2008), and in the Luzon Strait, with the maximum ^{137}Cs level occurring at 150 m depth (Zhou et al., 2018). In the outer shelf region, ^{137}Cs activity decreased with increasing depth at station E6, while in the estuary area, a reverse trend was observed at station C2 (Fig. 3b). At all stations in the YS, ^{137}Cs concentrations in the bottom layer were slightly lower than in the surface layer (Fig. 3c).

3.3. Grain size distribution of surface sediments

The mean grain size (φ, $\varphi = -\log_2^M$, M refers to mean grain size in mm) and percentage of clay component of surface sediments are listed in Table S2 and plotted in Fig. 4a and b. The mean grain size (φ) ranged from 2.0 to 7.9 and clay content ranged from 3.3% to 48.6%. In the ECS, sediment pattern is characterized by "fine-coarse-fine" feature from the inner shelf to shelf slope. In the Zhe-Min coast and the ECS shelf slope area, the clay contents were higher than 25% and sand contents were lower than 10%, while in the outer shelf region the sand content was larger than 60% and clay content was lower than 15%. In the southwestern Cheju island, the clay content was also higher than 25%. The highest clay content was found in the central YS with percentage >40%. The sand contents in this area were generally lower than 5%. In the north of the Yangtze estuary and the western part of the Southern YS, two small patches of coarse sediments composed of clay (<10%), silt (<25%) and sand (>65%) were observed. (See Fig. 4b.)

3.4. Spatial distribution of ^{137}Cs in surface sediments

The ^{137}Cs activity in surface sediments is listed in Table S2 and plotted in Fig. 4c. The ^{137}Cs activities in surface sediments of the ECS, YS and BS ranged between 0.30 and 5.22 Bq/kg (mean: 1.45 ± 1.00 Bq/kg), 0.54 and 5.02 Bq/kg (mean: 1.81 ± 1.09 Bq/kg) and 0.52 and 4.58 Bq/kg (mean: 1.57 ± 0.92 Bq/kg), respectively. In the ECS, ^{137}Cs activities varied by more than an order of magnitude. The highest values were observed in the Zhe-Min coastal area with a sharply decreasing trend offshore. The lowest activities were found in the outer shelf. Activities then increased slightly near the shelf slope area. In the central YS, a

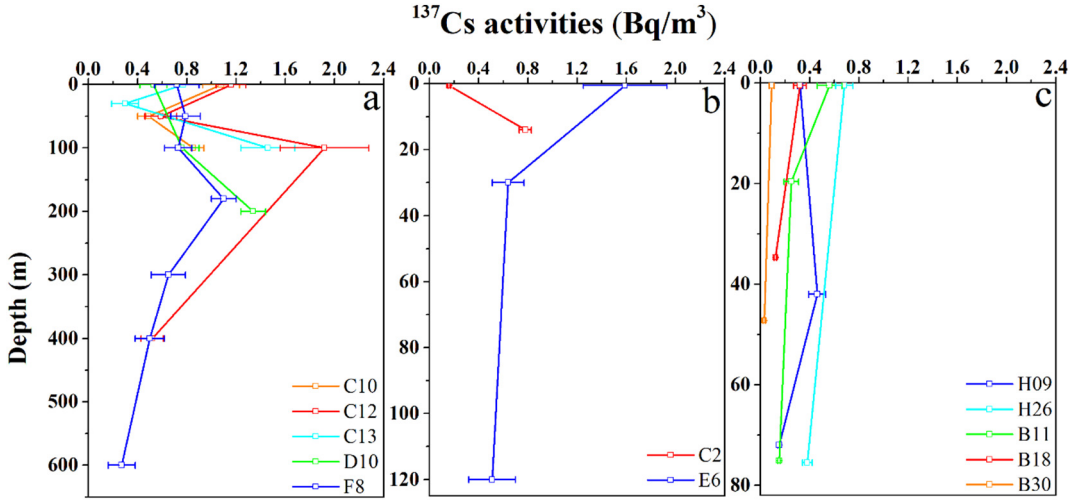

Fig. 3. Vertical profiles of ^{137}Cs activities in the water column of the ECSs.

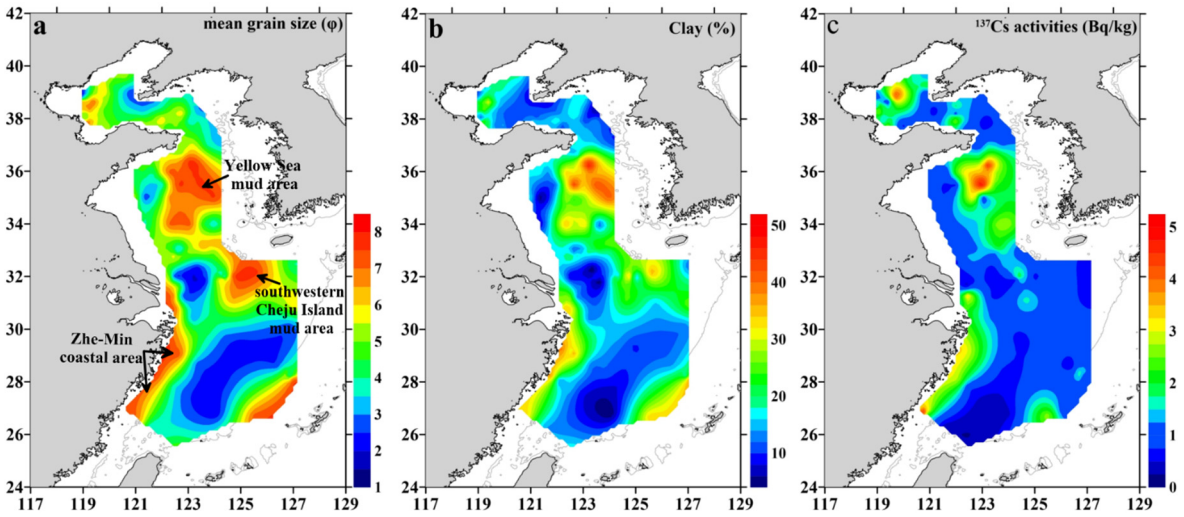

Fig. 4. Spatial distribution of mean grain size (φ), clay component (%) and ^{137}Cs activities (Bq/kg) in surface sediments of the ECSs.

large patch of high activity was observed. The high value region was also found in the central BS. In the western part of the YS and the BS strait, ^{137}Cs activities in surface sediments were very low. In general, the spatial distribution of ^{137}Cs activities in surface sediments was similar to the mean grain size pattern.

4. Discussion

4.1. Sources and sinks of ^{137}Cs in the ECSs

The major sources of ^{137}Cs in the ECSs are potentially from atmospheric fallout from global weapons testing, riverine input from the soil erosion, emission from the coastal nuclear power plants (NPPs), influence of the Fukushima accident and oceanic input from the WNP. The output of ^{137}Cs in the ECSs is burial to the seafloor sediments and natural decay. So far, there was no any report on the leakage of radionuclide contaminants from Chinese coastal NPPs, and sediment cores in the ECSs did not record the signal of such input of ^{137}Cs (Huh and Su, 1999; Li et al., 2013; Zhu et al., 2014; Liu et al., 2015). Besides, ^{137}Cs in coastal water of the ECSs was lower than offshore area, this observation further confirmed that the emission from the coastal NPPs could be negligible. The majority of the Fukushima accident-derived ^{137}Cs has been proved to be transported eastward (Buesseler et al., 2017), and in gamma spectrums of all samples we did not observe the signal of ^{134}Cs at 604 keV, thus the influence of the Fukushima accident could also be negligible.

4.1.1. Input from atmospheric fallout of ^{137}Cs

As a typical artificial radionuclide, the atmospheric fallout of ^{137}Cs is in a nonsteady state. Large-scale atmospheric nuclear weapons testing was conducted in 1961–1962, and the stratospheric residence time of ^{137}Cs was approximately 1 year. Accordingly, the annual deposition rate of ^{137}Cs peaked in 1963 (Hirose et al., 2008). Then, the deposition rate declined over time, except in 1986–1987 that was influenced by the Chernobyl accident. However, long-term observation in Tsukuba (36°03′N, 140°08′E) showed that the declining trend of the ^{137}Cs deposition slowed or almost ceased since the 1990s, suggesting that current ^{137}Cs deposition is boosted by the resuspension and transportation of ^{137}Cs deposited on the East Asian continent (Hirose et al., 2008). Since our study area is also located in the Asian yellow dust plume, it is expected that the current deposition status over the ECSs is similar to the observation in Tsukuba. Therefore, we use the mean value (0.22 ± 0.09 Bq/m^2/y) measured in Tsukuba during 1990–2010 as the current ^{137}Cs deposition rate in the ECSs. This value is comparable to the result (0.33 ± 0.20 Bq/m^2/y) obtained in Shanghai (31°13′39″ N, 121°23′56″ E) during 2006–2007 (Du et al., 2010). The surface areas of our study areas in the BS, YS, and ECS were estimated by Google Earth to be 0.33×10^5 km^2, 1.95×10^5 km^2 and 3.82×10^5 km^2, respectively. Multiplying by the ^{137}Cs deposition rate, the input of ^{137}Cs to the three seas by atmospheric fallout are calculated to be $(0.7 \pm 0.3) \times 10^{10}$ Bq/y, $(4.3 \pm 1.8) \times 10^{10}$ Bq/y and $(8.4 \pm 3.4) \times 10^{10}$ Bq/y, respectively.

4.1.2. Riverine input from the soil erosion in the catchment

There are many rivers around the ECSs, 40 of which are >1000 km^2 in catchment area. These rivers annually discharge tremendous amounts of terrestrial sediments into the ECSs and could be a potential source for the ^{137}Cs budget as a result of soil erosion in the drainage basin. Ideally, calculating a riverine contribution precisely should be based on field measurements in each river mouth. However, it is too massive of a project to carry out, and very few data of ^{137}Cs in river water have been published. Previous studies suggested that the riverine input of radionuclides can be roughly estimated by the following equation (modified from: Ravichandran et al., 1995; Baskaran et al., 1997):

$$I_d = A_d \times I_f \times f_e \quad (1)$$

where A_d is the area of the drainage basin, I_f is the reference inventory of radionuclide in soils (Bq m^{-2}), and f_e is the fraction of radionuclide eroded each year from drainage basin (f_e = ln2/residence time of radionuclide in drainage basin). This method has been applied successfully in the ECS to estimate the input of ^{210}Pb and $^{239+240}$Pu derived from the Yangtze River (Su and Huh, 2002; Wang et al., 2017a).

As shown in the equation, the riverine input contribution depends on the catchment area and residence time of the radionuclide in the drainage basin. The residence time of ^{137}Cs in several different scale catchments has been investigated, with the value reported to be 800 y in the Rhone River (catchment area: 0.52×10^4 km^2), 1500 y in the Saguenay River (7.8×10^4 km^2) and 4100 y in the Columbia River (68×10^4 km^2) (Smith and Ellis, 1982; Dominik et al., 1987; Beasley and Jennings, 1984). If the catchment area is larger, the corresponding residence time is longer. Therefore, the ^{137}Cs input from small rivers may not be neglectable. Considering massive catchment areas and the construction of many dams (e.g., the Three Gorges Dam and the Xiaolangdi Dam), we use the largest value of 4100 y as the residence time of ^{137}Cs in the Yangtze River and the Yellow River. For other small rivers around the ECSs, the ^{137}Cs residence time assignment depends on their catchment areas (Table S3). ^{137}Cs has been widely applied in determining soil erosion rates in mainland China and the Korean Peninsula (e.g. Zhang et al., 2003; Zhang et al., 2011; Meusburger et al., 2013; Ma et al., 2016; Li et al., 2017). As a consequence, there is an available

comprehensive dataset of ^{137}Cs reference inventories in soils (Table S4), which enables us to better estimate the riverine input of ^{137}Cs. The ^{137}Cs inventories in high latitudes (30°N-40°N) are generally higher than those in low latitudes (20–30°N), which is consistent with global fallout patterns.To calculate riverine inputs, we divide the ^{137}Cs inventory data into four parts, and the corresponding arithmetic mean value in each part is shown in Fig. 5. The mean ^{137}Cs inventory in the Yellow River basin is 1594 ± 251 Bq/m^2, and accordingly, the input of ^{137}Cs from the Yellow River is estimated to be (2.0 ± 0.3) × 10^{11} Bq/y. The Yellow River discharge is approximately 0.7 × 10^8 tons/y of terrestrial sediments into the BS (CWRC, 2014). Thus, the mean ^{137}Cs activity in suspended particulates eroded from the drainage basin can be calculated to be 2.9 ± 0.5 Bq/kg. This value is close to the activity of surface sediments near the Yellow River mouth. The Yangtze River delivers the most terrestrial ^{137}Cs into the ECS. The mean ^{137}Cs inventory in the Yangtze catchment is 1462 ± 470 Bq/m^2. Thus, the riverine input is calculated to be (4.5 ± 1.4) × 10^{11} Bq/y. However, this estimation is eight times larger than the filed measured value (0.51 × 10^{11} Bq/y) at the Xuliujing station (Du et al., 2010). The discrepancy may come from two aspects. First, the field measurement was carried out in 2006–2007, when the Yangtze basin runoff was at its lowest level in the last half century due to extremely low annual rainfall, high temperatures and the impounding of Three Gorges Dam from 135 m to 156 m (Dai et al., 2008). The global fallout of ^{137}Cs should be much higher in the 1960s compared to 2006–2007, which lead to a much higher riverine discharge of ^{137}Cs in the 1960s. Thus, it is not surprising that our estimated result represents a mean value between 1952 and 2013 and is higher than the measured value during 2006–2007. Second, the residence time of ^{137}Cs in the Yangtze basin is a highly uncertain factor, even though we used the largest value of the range (4100 y), the residence time might still be underestimated and the input of ^{137}Cs might be overestimated. Taking all rivers into the calculation (Table S3), the total riverine inputs to the BS, YS and ECS were estimated to be (5.1 ± 0.4) × 10^{11} Bq/y, (2.0 ± 0.2) × 10^{11} Bq/y and (5.7 ± 1.3) × 10^{11} Bq/y, respectively.

4.1.3. Sediment accumulation rates and ^{137}Cs burial

In the past few decades, the sediment accumulation rate estimated by radioisotopes (^{210}Pb, ^{137}Cs and $^{239+240}$Pu), as an important factor in sedimentary process studies in the ECSs, has been intensely investigated (e.g. DeMaster et al., 1985; Alexander et al., 1991; Li et al., 1993, 2006; Huh and Su, 1999; Su and Huh, 2002; Oguri et al., 2003; Fang et al., 2007; Li et al., 2013; Qiao et al., 2017). The highest sediment accumulation rates (>2 cm/y) are observed near the Yangtze River mouth and the Yellow River mouth (Fig. 6a). In the coastal and inner shelf of the ECS, sediment accumulation rates are high but decrease eastward sharply to <0.1 cm/y. Well-preserved sedimentary structures in the coast and inner shelf suggest that sediment deposition is dominant compared to other factors, even though remobilization and resuspension of sediments are active (McKee et al., 1983; DeMaster et al., 1985; Wang et al., 2016). Moreover, sediment accumulation rates derived from different radioisotopes showed a high consistency, indicating that biological perturbation is limited (DeMaster et al., 1985; Su and Huh, 2002). The sediment accumulation rates in the YS are generally low, with a decreasing trend from west to east. Relatively high rates in the western part are a result of sediment input eroded from the old Yellow River delta (Alexander et al., 1991). In the modern Yellow River delta front region, the accumulation rates decline from above 2 cm/y to below 0.2 cm/y with a sharp gradient.

At the same interpolation gridding density, by combining ^{137}Cs activities in surface sediments, bulk density and sediment accumulation rates, the spatial distribution of ^{137}Cs burial flux in surface sediments in the ECSs can be obtained (Fig. 6b). There are two patches of high ^{137}Cs burial flux. The first patch of high ^{137}Cs burial flux is located in the coastal area along the sediment dispersal path of the Yangtze River, with a sharply decreasing trend offshore. Such a narrow band with a high ^{137}Cs burial flux reveals that most of the terrestrial ^{137}Cs was carried by the Yangtze River deposits in the estuary and inner shelf area. The second patch of high ^{137}Cs flux is found in the Yellow River delta, with a maximum value above 200 Bq/m^2/y. These observations support the fact that riverine input makes important ^{137}Cs

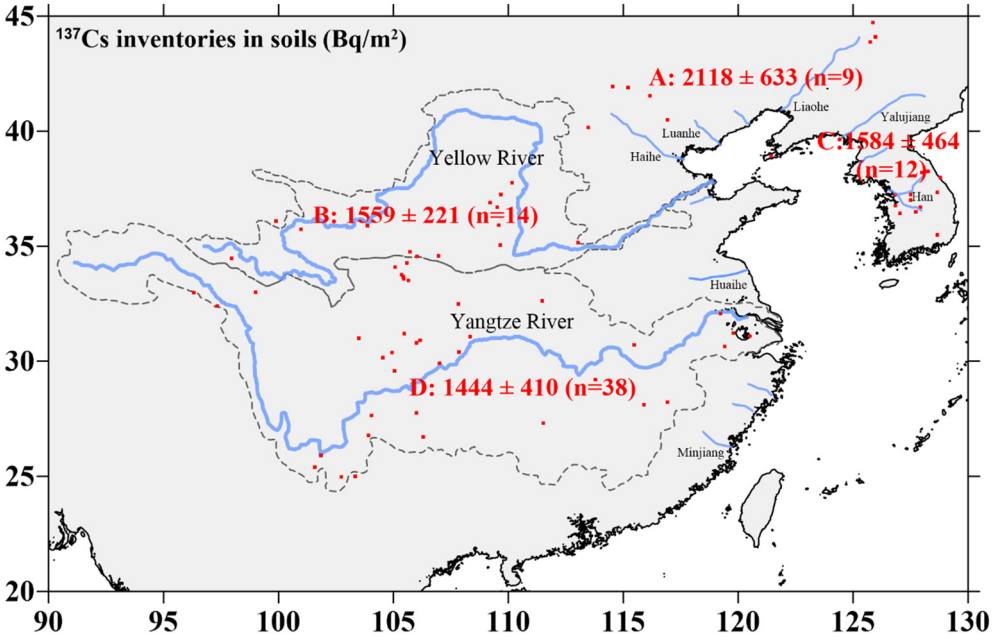

Fig. 5. The synthesis of decay-corrected ^{137}Cs inventory (Bq/m^2) in river drainage basin surrounding the ECSs. The red symbols show locations of soil cores in published literatures and the details of ^{137}Cs inventory data are summarized in Table S4 (Menzel et al., 1987; Zhang et al., 1990, 1994, 1997, 1998, 2003, 2006; Quine et al., 1992; Li et al., 1993, 1995; Lee et al., 1996; Lu and Higgitt, 2000; Cao et al., 2001; Zhang et al., 2002, 2011; Jin et al., 2004; Pu et al., 2004; Yan and Shi, 2004; Zhang et al., 2004; Hu et al., 2005; Yan and Yang, 2005; Zhao et al., 2005; Fang et al., 2006; Hua et al., 2006; Tang et al., 2006; Zheng et al., 2007; Yan et al., 2008; Li et al., 2009b; Li et al., 2009a; Zhang et al., 2009b; Jiang, 2010; Zhang et al., 2010; Shao et al., 2011; Wang et al., 2011; Yang et al., 2011; Jia et al., 2012; Meusburger et al., 2013; Liang et al., 2014; Wang et al., 2014; Zhang et al., 2014; Li et al., 2015; Xu et al., 2015; Zhang et al., 2015; Ma et al., 2016; Li et al., 2017; Su et al., 2017). For calculating the riverine input, four parts are divided and corresponding arithmetic mean value is shown. Part A: Haihe–Liaohe basin; Part B: Yellow River basin; Part C: Korean Peninsula; Part D: Yangtze River basin.

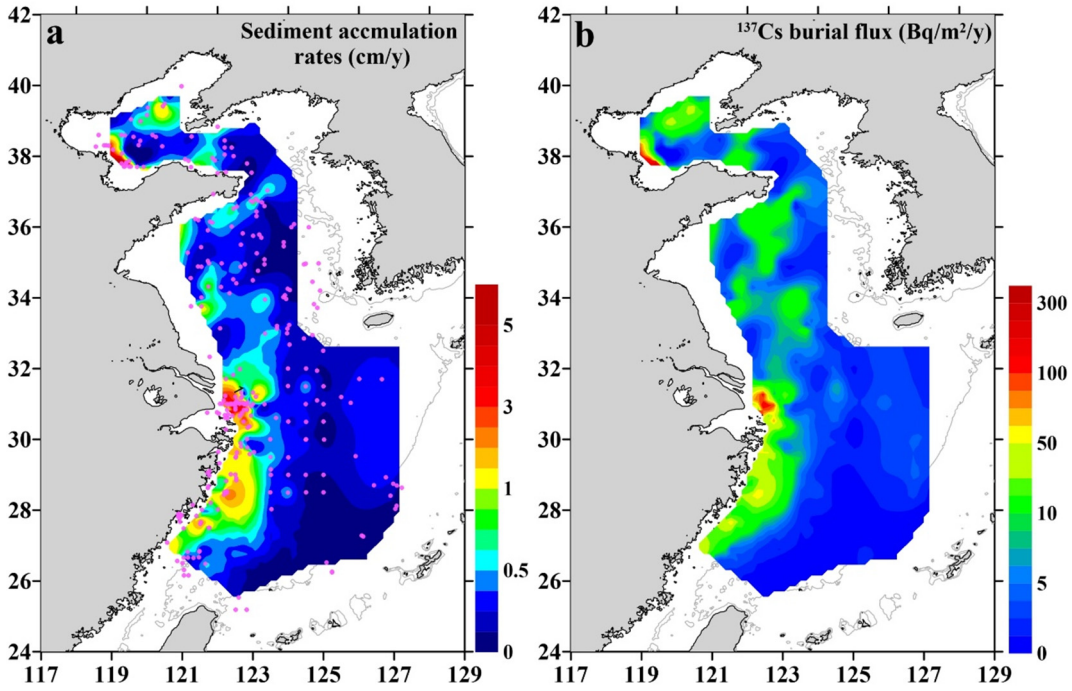

Fig. 6. Sediment accumulation rates (cm/y) and ^{137}Cs burial flux (Bq/m^2/y) in the ECSs. The purple symbols show locations of sediment cores in published literatures and the details of sediment accumulation rates are summarized in Table S5 (DeMaster et al., 1985; Zhao et al., 1991; Alexander et al., 1991; Yang et al., 1993; Xie et al., 1994; Chung and Chang, 1995; Huh and Chen, 1999; Huh and Su, 1999; Xia et al., 1999, 2004; Lin et al., 2000; Li et al., 2002, 2006; Su and Huh, 2002; Oguri et al., 2003; Chen et al., 2004; Zhang et al., 2005; Liu et al., 2006; Fang et al., 2007; Guo et al., 2007; Lim et al., 2007; Yang and Youn, 2007; Yang and Chen, 2007; Zhang et al., 2009a; Dong et al., 2009; Feng et al., 2009; Liu et al., 2009; Zhang et al., 2009c; Hu et al., 2011a; Gao et al., 2011; Liu and Fan, 2011; Youn and Kim, 2011; Wen, 2012; Duan et al., 2013; Li et al., 2013; Zhu et al., 2014; Liu et al., 2015; Hu et al., 2016; Zhou et al., 2016; Wang et al., 2017a; Qiao et al., 2017; Lin et al., 2018; Xu et al., 2018).

contributions in the estuary areas. The ^{137}Cs activities and sediment accumulation rates in the outer shelf of the ECS are both low, and thus, the ^{137}Cs burial flux is very low. The weighted averages of ^{137}Cs burial fluxes to surface sediments in the BS, YS and ECS are calculated to be approximately 22.4 ± 8.7 Bq/m^2/y, 6.9 ± 1.6 Bq/m^2/y, and 7.3 ± 2.3 Bq/m^2/y, respectively. Accordingly, the total ^{137}Cs burial fluxes can be estimated to be (7.4 ± 2.9) × 10^{11} Bq/y, (1.3 ± 0.3) × 10^{12} Bq/y and (2.8 ± 0.9) × 10^{12} Bq/y in the BS, YS and ECS, respectively. The ^{137}Cs burial fluxes in the YS and ECS are far greater than the riverine input and atmospheric fallout, which suggests that the dominant source of ^{137}Cs in the YS and the ECS is oceanic input from the WNP by the KC, although riverine input is important for the estuary areas.

4.2. ^{137}Cs budget in the ECSs

In a given region, ^{137}Cs activity in the water column is determined by external input (atmospheric fallout, riverine input and oceanic input) and output (sedimentary deposition and natural decay). Therefore, the temporal change of ^{137}Cs inventory can be expressed by a box model:

$$dI/dt = R_{Cs} + A_{Cs} + O_{Cs} - \lambda \times I - B_{Cs} \quad (2)$$

where I is the inventory of ^{137}Cs in the water column (Bq), λ (0.023 y^{-1}) is the natural decay constant of ^{137}Cs, and R_{Cs}, A_{Cs}, O_{Cs} and B_{Cs} refer to the riverine input (Bq/y), atmospheric fallout flux (Bq/y), net oceanic contribution and burial flux into surface sediments (Bq/y), respectively. The R_{Cs}, A_{Cs}, and B_{Cs} have been discussed above, but the temporal change of ^{137}Cs inventory (dI/dt) still needs to be solved. Under steady-state conditions, the ^{137}Cs inventory remains constant over time such that dI/dt is equal to zero. However, exponentially decreasing trends over time of ^{137}Cs activity in surface seawaters have been observed in many seas such as the Japan Sea (Kasamatsu and Inatomi, 1998) and the Pacific Ocean (Hirose and Aoyama, 2003). The historical data of ^{137}Cs in the surface water of the YS and ECS are plotted against time in Fig. 7. The ^{137}Cs data are fitted to exponentially decreasing curves, and the apparent half-lives of ^{137}Cs are estimated to be 15.1 y for the ECS and 7.7 y for the YS. The value obtained in the ECS is slightly lower than those found in the Japan Sea (18.7 y) (Kasamatsu and Inatomi, 1998), the South China Sea (16.9 y) (Wu, 2018) and the Northwest Pacific Ocean (17 y) (Hirose and Aoyama, 2003). Unfortunately, the data in the BS are so rare that we only can use the value estimated in the YS as a compromise. The ^{137}Cs inventory at each vertical profile can be calculated by integrating ^{137}Cs activities at each depth (Ito et al., 2003):

$$I = \frac{1}{2}\left\{\sum_{i=1}^{N}(C_i + C_{i+1})(d_{i+1} - d_i) + 2C_1 d_1 + 2C_N(d_B - d_N)\right\} \quad (3)$$

where I is ^{137}Cs inventory (Bq/m^2), N is the number of sampling depths, C_i is the ^{137}Cs activities at depth I (Bq/m^3), di is the ith sampling depth (m), d_1 is the first sampling depth (m), and d_B is the total depth to the bottom (m). Using this formula and surface area of the YS (1.95 × 10^5 km^2), we can calculate that the ^{137}Cs inventories in the YS is (3.8 ± 3.0) × 10^{12} Bq. For the BS, considering its water depth is shallow, we assume the concentration of ^{137}Cs in the water profiles of the Bohai Sea is homogeneous, and thus we use the ^{137}Cs concentration in surface water to calculate that the ^{137}Cs inventories in the BS is (3.8 ± 2.0) × 10^{10} Bq. In the ECS, we divide it into two parts (shallow waters (<100 m) and deep waters) to calculate ^{137}Cs inventories. For the shallow waters, we assume the concentration is homogeneous in vertical distribution. For the deep waters part, we use the vertical profiles to estimate the ^{137}Cs inventory. Finally, the ^{137}Cs inventory in the ECS water is calculated to be (5.1 ± 3.3) × 10^{13} Bq (details are shown in supplemental file). Combining the apparent half-lives and ^{137}Cs inventories in the water column, the dI/dt in the BS, YS and ECS are estimated to be (0.3 ± 0.2) × 10^{10} Bq/y, (3.3 ± 2.6) × 10^{11} Bq/y and (2.4 ± 1.5) × 10^{12} Bq/y, respectively.

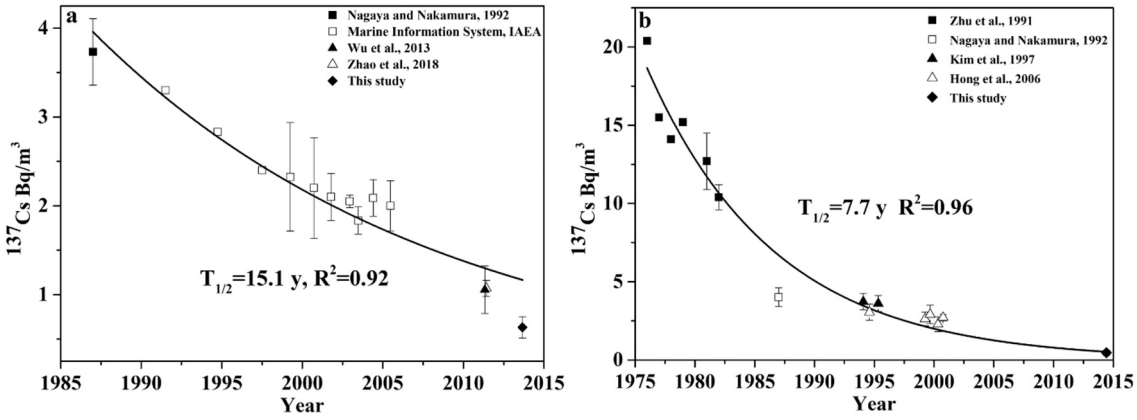

Fig. 7. Temporal changes of ^{137}Cs activities in surface seawater of the ECS (a) and YS (b) during the past few decades (Zhu et al., 1991; Nagaya and Nakamura, 1992; Kim et al., 1997; Hong et al., 2006; Wu et al., 2013; Zhao et al., 2018; MARIS data are from http://maris.iaea.org/Home.aspx).

Finally, using the box model, the interlinked budget balance of ^{137}Cs between the BS, YS and ECS is constructed (Fig. 8). The BS is a typical semienclosed sea and connect to the YS only through the Bohai Strait; thus, it is an ideal model for a box calculation and can be served as a starting point for budget calculation. The net oceanic input for the BS is calculated to be $(2.2 \pm 2.9) \times 10^{11}$ Bq/y, and this value actually is the ^{137}Cs outflow flux from the YS to the BS. Subtracting the outflow flux from the budget calculation of the YS, the ^{137}Cs input from the ECS to the YS is calculated to be $(1.7 \pm 0.4) \times 10^{12}$ Bq/y. Likewise, about $(7.4 \pm 1.9) \times 10^{12}$ Bq/y of ^{137}Cs should be transported from the WNP to the ECS, this value is very close to the previously estimated result (7.7×10^{12} Bq/y) obtaining by compartment model POSIDON-R (Maderich et al., 2014). Apparently, the oceanic input from the open ocean is a dominant source for ^{137}Cs in the ECSs, and the oceanic input is 5.2 times higher than the sum of the riverine input and atmospheric fallout. Considering the fact that we might overestimate the riverine input of ^{137}Cs, the result reported here should be a conservative estimation.

The KC brings approximately 7.9×10^{14} m^3 y^{-1} of high salinity water to the ECS (Kagimoto and Yamagata, 1997). In this study, the mean ^{137}Cs activity in the 100–200 m layer of the KC is calculated to be 1.3 ± 0.4 Bq/m^3. Multiplying the flow of the KC into the ECS and mean ^{137}Cs activity, we can roughly estimate that $(10.3 \pm 3.2) \times 10^{14}$ Bq/y of ^{137}Cs passes through the ECS. Therefore, the trapped ^{137}Cs in the ECSs accounts for 0.7% ± 0.3% (calculated by dividing the total ^{137}Cs of 10.3×10^{14} Bq/y passing through the ECS by the net oceanic input into the ECS of 7.4×10^{12} Bq/y) of the total ^{137}Cs transported by the KC. Among the oceanic inputs of ^{137}Cs, approximately 20% can be transported into the YS. However, only 3% can reach into the BS.

4.3. Implication of ^{137}Cs use for tracing water mass movement and exchange

In the estuarine regions, ^{137}Cs can be removed from the water body by adsorbed on the clay particles due to higher SPM concentration. However, due to very low K_d value of ^{137}Cs (<500 L/kg) in seawater and relatively lower SPM concentration (<10 mg/L) of shelf waters, ^{137}Cs is highly soluble and can be used to trace water mass movement in shelf waters. Though there have been many studies using ^{137}Cs as a tracer for water mass movement all over the world's oceans (e.g. Bowen et al., 1980; Aarkrog et al., 1983; Povinec et al., 2011; Aoyama et al., 2008, 2011), most studies focus on the open ocean, not marginal seas. For the sake of clarity, we summarize the salinity and temperature ranges of water masses in the ECSs and plot the ^{137}Cs activities in a T-S diagram (Fig. 9). In the ECS (Fig. 9a), different color spots show blocky distribution characteristics. Low ^{137}Cs activities were found in the Yangtze Estuary and extended to the northeast to Cheju Island due to the large amount of freshwater discharge and low ^{137}Cs wash out from the catchment area. In freshwater, ^{137}Cs is highly particle-reactive, with a K_d value of approximately 10^5 L/kg (Baskaran et al., 2015; Wang et al., 2017b), and low levels of dissolved ^{137}Cs have been found in the Yangtze River water (Du et al., 2010). The mean ^{137}Cs activity of the ECS water (0.62 ± 0.32 Bq/m^3) in summer was lower than that in our previous report (1.07 ± 0.09 Bq/m^3) during May 2011 (Zhao et al., 2018). The discrepancy was mainly derived from the influence of the seasonal variation of the CDW. Moreover, the low ^{137}Cs region in spring appeared in the southeast of the Yangtze Estuary and the Zhe-Min coast (Zhao et al., 2018). The distinct difference in the low ^{137}Cs region is in line with the dispersal path of the CDW in different seasons. During the flood season, the CDW flows toward the northeast and may extend to Cheju Island, while in the dry season, the CDW flows southward in a narrow band confined to the Zhe-Min coast (Wu et al., 2011, 2014). Thus, ^{137}Cs could respond precisely to the seasonal variation of the CDW plume.

High ^{137}Cs activities were observed in the Kuroshio surface water (KSW) and the Kuroshio subsurface water (KSSW), which supports the fact that the oceanic input from the WNP is a dominant source of ^{137}Cs in the ECS. The residence time of the ECS shelf water has been proven to be 1.3 ± 0.27 y (Wang et al., 2018c). Thus, the material exchange between the ECS and the WNP through shelf-edge intrusion of the KC is active (Wong et al., 2000). The massive intrusion mainly occurred northeast of Taiwan Island due to topographic deflection and is

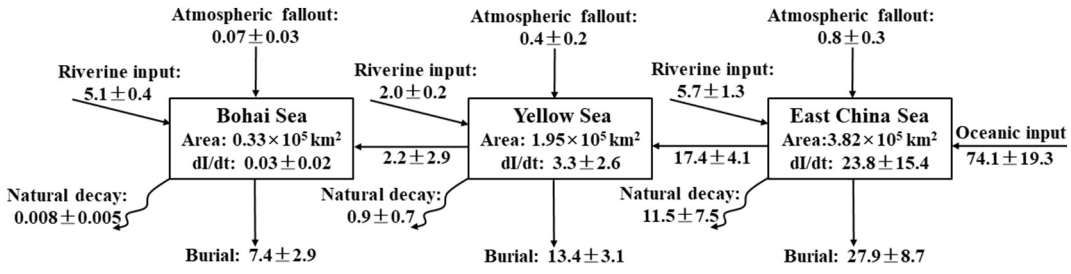

Fig. 8. Interlinked budget balance of ^{137}Cs (10^{11} Bq/y) between the BS, YS and ECS.

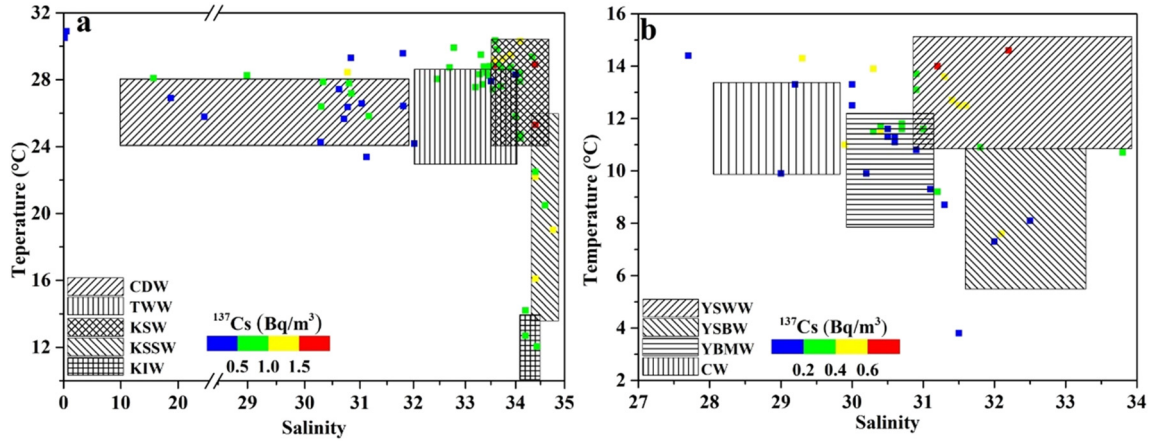

Fig. 9. ^{137}Cs activities of seawater samples plotted in T-S diagram. Different colors represent ^{137}Cs activities, note difference in scale of color bar. The temperature and salinity range of water masses in the ECSs is from previous study (Liu et al., 1993; Hur et al., 1999; Chen, 2009; Qi et al., 2014). CDW: Changjiang Diluted Water; KSW: Kuroshio Surface Water; KSSW: Kuroshio Subsurface Water; KIW: Kuroshio Intermediate Water; TWW: Taiwan Warm Water; YSWW: Yellow Sea Warm Water; YSBW: Yellow Sea Bottom Water; YBMW: Yellow-Bohai Sea Mixed Water; CW: Costal water.

a year-round phenomenon, characterized by the upwelling of the KSSW (Liu et al., 1992; Wong et al., 2000). In addition, small-scale intrusions in the form of frontal eddies could occur along the ECS shelf edge (Yanagi et al., 1998). Therefore, the intrusion of the KSSW is a main mechanism of ^{137}Cs import into the ECSs. The ^{137}Cs vertical profiles near the shelf edge further confirms our hypothesis (Fig. 3c). Among five stations located along the ECS shelf edge, the maximum values were observed in the subsurface layer at a water depth of 100–200 m in four vertical profiles of ^{137}Cs (F8, D10, C12 and C13). On the basis of numerical simulation and field observations, Yang et al. (2012) suggested that the KSSW could intrude near the Yangtze river mouth via the bottom layer. Similar results were also obtained using δ^{18}O, δD and ^{129}I/^{127}I as tracers (Lian et al., 2016; Wang et al., 2018a). In this study, at station C2, the ^{137}Cs level in the bottom layer was approximately five times higher than that in the surface layer. The high ^{137}Cs concentration in the bottom layer near the Yangtze River mouth is a clear signal of the intrusion of the KSSW. In the north of the ECS, the relatively high ^{137}Cs level showed a mixing between the KC/TWC waters and the CDW water. This result indicates that a portion of ^{137}Cs could be transported to the YS from the ECS via the YSWC, which is consistent with the budget calculation as discussed above.

Regarding the YS-BS (Fig. 9b), relatively high ^{137}Cs activities were observed in the Yellow Sea Warm Water (YSWW). The high ^{137}Cs level decreased sharply northward, but smoothly westward (Fig. 2b). Such a distribution pattern suggests that the YSWC does not exactly flow along the YS trough but is displaced significantly westward. The westward shift of the YSWC has already been pointed out in several previous studies (Xie et al., 2002; Huang et al., 2005; Ma et al., 2006; Lin et al., 2011). The warm water intrusion can reach approximately 122.5°E at 35°N; then, a large portion turns to northeast, but a small warm water tongue continues trending northwestward to the Shandong coast (Lin et al., 2011). The BSCC carries extremely low ^{137}Cs water into the YS and then meets the YSWW. Thus, the lower ^{137}Cs south of the Shandong Peninsula might be a result of mixing between the YSWC water and the BSCC water. According to our mass balance calculation, only 4% of ^{137}Cs is derived from oceanic input, therefore, the lower ^{137}Cs activity in the BS surface waters should be attributed to the low concentration in the Yellow River and other rivers. In addition, the spatial distribution of ^{137}Cs in the surface water with low values in May 2014 suggests that in spring, the YSWC only intrudes into the southern YS and eastern part of the northern YS but not into the BS. The 4% of oceanic input of ^{137}Cs to the BS should be contributed by YSWC transport in winter (Guan, 1994).

Overall, the spatial and vertical distribution of ^{137}Cs is significantly controlled by the complex current system in the ECSs. The high level of ^{137}Cs in oceanic water masses and low level of ^{137}Cs in riverine and coastal waters make ^{137}Cs a good indicator for tracing water mass movement and interaction in the ECSs. It has been reported that KSSW is rich in nutrients, especially phosphate (Liu et al., 2000; Zhang et al., 2007); thus, the results in this study are expected to help us to understand nutrient transport and budgets in the ECSs.

4.4. Implication of ^{137}Cs as a tracer for sediment transport in river-dominated margins

In freshwater, ^{137}Cs is preferentially adsorbed by clay minerals (especially illite) and is strongly associated with cation-exchange sites (Duran et al., 2004). Once these clay particles were discharge to the sea, the desorption of ^{137}Cs from particles was reported to be small, with a maximum value of 9% (Takata et al., 2015). Ohnuki and Kozai (2013) investigated the desorption of ^{137}Cs and found that it was <20% even when leaching with 1 M HCl. Thus, ^{137}Cs in clay matrices is nearly immobile and can be transported in pace with the terrestrial fine sediments in river-dominated marginal seas. The sediments from the Yangtze River and Yellow River are abundant with fine particles, and mean grain size (φ) of suspended particles in the Datong station and Lijin station were documented to be 6.64 and 5.72, respectively (CWRC, 2014). In addition, X-ray diffraction analysis demonstrated that illite is the most abundant clay mineral in both sediments from the Yangtze River and the Yellow River (~70% and ~60%, respectively) (Fan et al., 2001; Wang and Yang, 2013). Thus, the majority of suspended sediments, especially fine particles, originating from the Yangtze River and Yellow River are tagged with ^{137}Cs. These ^{137}Cs-tagged sediments deposit predominantly in river mouths at first, and subsequently, a large portion of deposited sediments is eroded, and resuspension then disperses throughout the entire ECSs by following the coastal currents.

In the Yangtze River mouth, the difference between short- and long-term sedimentation rates, 4 cm/month versus 1–5 cm/year, suggests that a large proportion of sediment are eroded on a seasonal basis and transported farther offshore (McKee et al., 1983) that corresponds to the southward alongshore dispersion of fine sediments as revealed by the low mean grain size and high ^{137}Cs activity. The outer shelf of the ECS was covered by coarse sand due to the relict sediment deposition during the last glacial period (Qin et al., 1996), and thus, the ^{137}Cs in the outer shelf is lower. Near the shelf edge of the ECS, relatively high

activities are also observed. Previous studies have revealed that suspended sediments can be transported from the inner shelf to the shelf edge in the autumn and winter (Yanagi et al., 1996; Iseki et al., 2003; Wang et al., 2018b). The near-bottom transport is the dominant mechanism of sediments across the shelf, as proven by the total suspended material profile along the PN section (Deng et al., 2006). Therefore, relatively high activities near the shelf edge of the ECS are a result of the across-shelf transport of sediments. The extremely high ^{137}Cs levels with a decreasing trend southward coincide with the southward dispersion of fine particles discharged from the Yellow River. Fine sediments from the Yellow River can travel via the BSCC through the Bohai Strait into the YS. Due to the cyclonic gyre upwelling/downwelling, most of these sediments are deposited in the central Yellow Sea (Lee and Chough, 1989; Alexander et al., 1991; Lim et al., 2007; Yang and Youn, 2007). Previous studies suggested that the fine sediments in the southwestern Cheju Island mud area are derived from the Yangtze River, Yellow River, and erosion of the old Yellow River delta along the north Jiangsu coast (Milliman et al., 1985; Alexander et al., 1991; Liu et al., 2003; Lim et al., 2007). The sediments from the Yangtze River and the Yellow River both have high ^{137}Cs activities, but ^{137}Cs in the old Yellow River delta is presumably low because there was no ^{137}Cs before 1855. If contributions from the three sources are approximately the same, the ^{137}Cs activity should be relatively high. Therefore, the low ^{137}Cs in the southwestern Cheju Island mud area might indicate that it was mainly originated from the old Yellow River delta, but not from the Yangtze River and Yellow River, at least after 1960's.

The ^{137}Cs activity in surface sediments is plotted against mean grain size (Fig. 10), that shows a good correlation. In the Kara Sea of the Russian Arctic, a positive correlation was also observed (Baskaran et al., 1996). The good correlation between ^{137}Cs activity and mean grain size further indicates that ^{137}Cs can be used as an effective tracer to track the dispersal pathways of fine sediments derived from the Yangtze River and Yellow River, even in a very complex and dynamic system. It has been reported that riverine input sediments can carry many other particle-active pollutants. Lin et al. (2002) pointed out that heavy metals, such as Fe, Zn and Cu, are easily adsorbed by fine sediments. Hu et al. (2011b) found positive correlations between mean grain size and concentrations of dichlorodiphenyltrichloroethanes (DDTs) and hexachlorocyclohexanes (HCHs) in surface sediments in the YS. Therefore, the particle effect of ^{137}Cs is not only helpful to track the dispersal pathways of fine sediments but also useful to understand the transport processes and ultimate fates of other particle-reactive pollutants.

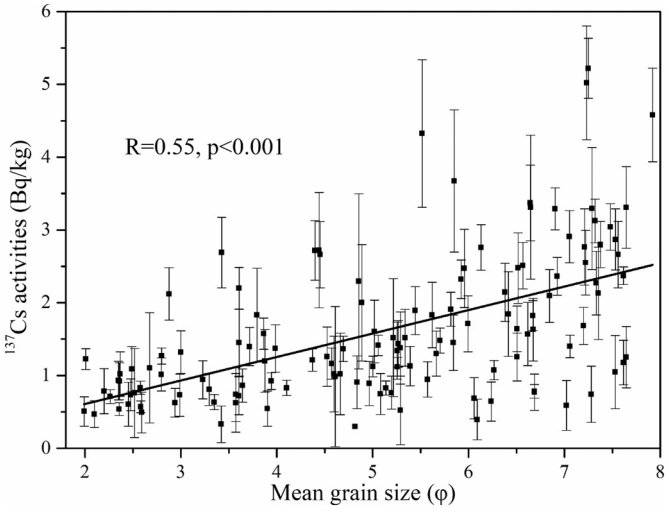

Fig. 10. The correlation diagram between mean grain size (φ) and ^{137}Cs activities (Bq/kg) of surface sediments.

5. Conclusion

We have measured ^{137}Cs activity in the water column and surface sediments of the ECSs. At the same time, the ^{137}Cs inventory data from land surfaces as well as sediment accumulation rates have been collected to evaluate riverine input and ^{137}Cs burial. ^{137}Cs activities in the ECSs water ranged from 0.03 to 1.92 Bq/m^3 with high ^{137}Cs observed in the shelf edge areas and low ^{137}Cs observed in the estuary and coastal areas. In surface sediments, ^{137}Cs activities ranged from 0.30 to 5.22 Bq/kg, with a high activity observed in the Zhe-Min coast and the central YS mud area. There was no ^{134}Cs signal in any samples, suggesting that the impact of the Fukushima accident on the ECSs was very limited. Using the ^{137}Cs inventory data of drainage basin and sediment accumulation rates over the ECSs, the total riverine inputs and ^{137}Cs burial fluxes into surface sediments are estimated to be $(1.3 \pm 0.1) \times 10^{12}$ Bq/y and $(4.8 \pm 1.0) \times 10^{12}$ Bq/y. Mass balance calculations show that the oceanic input from the open ocean is a dominant source for ^{137}Cs in the ECSs that is 5.2 times higher than the sum of the riverine input and atmospheric fallout.

The vertical profiles of ^{137}Cs with a maximum at a water depth of 100–200 m in the continental shelf edge and much higher ^{137}Cs in bottom waters compared to surface waters in the Yangtze Estuary reveal that the upwelling of the Kuroshio subsurface water is the main mechanism of ^{137}Cs import into the ECSs. The spatial distribution of ^{137}Cs suggests that in spring, the YSWC can intrude into the southern YS and east part of the northern YS but not into the BS. The high level of ^{137}Cs in oceanic water masses and low level of ^{137}Cs in riverine and coastal waters make ^{137}Cs a good indicator for tracing water mass movement and interaction in the ECSs. The fine grain size and low ^{137}Cs of surface sediments in the southwest region of Cheju Island suggest that the source of these regional sediments is dominated by old Yellow River delta input. There is a good correlation between ^{137}Cs activity and mean grain size (φ) in surface sediments, suggesting that ^{137}Cs can serve as an effective tracer to track dispersal pathways of fine sediments and associated particle-reactive pollutants in river-dominated marginal seas.

Acknowledgments

This research was supported by the National Natural Science Foundation of China (41706089) and China Postdoctoral Science Foundation (2017M610238). We would like to thank Jianan Liu and Xiaogang Chen for their kind help in the field sampling. We also wish to thank Associate Editor, Dr. Mae Sexauer Gustin and two anonymous reviewers for their constuctive comments for improvement of the original manuscript.

Appendix A. Supplementary data

Supplementary data to this article can be found online at https://doi.org/10.1016/j.scitotenv.2019.04.001.

References

Aarkrog, A., 2003. Input of anthropogenic radionuclides into the World Ocean. Deep-Sea Res. II Top. Stud. Oceanogr. 50 (17–21), 2597–2606.
Aarkrog, A., Dahlgaard, H., Hallstadius, L., Hansen, H., Holm, E., 1983. Radiocaesium from Sellafield effluents in Greenland waters. Nature 304 (5921), 49–51.
Alexander, C.R., DeMaster, D.J., Nittrouer, C.A., 1991. Sediment accumulation in a modern epicontinental-shelf setting: the Yellow Sea. Mar. Geol. 98 (1), 51–72.
Aoyama, M., Hirose, K., 1995. The temporal and spatial variation of ^{137}Cs concentration in the western North Pacific and its marginal seas during the period from 1979 to 1988. J. Environ. Radioact. 29 (1), 57–74.
Aoyama, M., Hirose, K., Igarashi, Y., 2006. Re-construction and updating our understanding on the global weapons tests ^{137}Cs fallout. J. Environ. Monit. 8 (4), 431–438.
Aoyama, M., Hirose, K., Nemoto, K., Takatsuki, Y., Tsumune, D., 2008. Water masses labeled with global fallout ^{137}Cs formed by subduction in the North Pacific. Geophys. Res. Lett. 35 (1). https://doi.org/10.1029/2007GL031964.
Aoyama, M., Fukasawa, M., Hirose, K., Hamajima, Y., Kawano, T., Povinec, P.P., Sanchez-Cabeza, J.A., 2011. Cross equator transport of ^{137}Cs from North Pacific Ocean to South Pacific Ocean (BEAGLE2003 cruises). Prog. Oceanogr. 89 (1–4), 7–16.

Aoyama, M., Hamajima, Y., Hult, M., Uematsu, M., Oka, E., Tsumune, D., Kumamoto, Y., 2016. ^{134}Cs and ^{137}Cs in the North Pacific Ocean derived from the March 2011 TEPCO Fukushima Dai-ichi Nuclear Power Plant accident, Japan. Part one: surface pathway and vertical distributions. J. Oceanogr. 72 (1), 53–65.

Baskaran, M., Asbill, S., Santschi, P., Brooks, J., Champ, M., Adkinson, D., Makeyev, V., 1996. Pu, ^{137}Cs and excess ^{210}Pb in Russian Arctic sediments. Earth Planet. Sci. Lett. 140 (1–4), 243–257.

Baskaran, M., Ravichandran, M., Bianchi, T.S., 1997. Cycling of ^{7}Be and ^{210}Pb in a high DOC, shallow, turbid estuary of South-east Texas. Estuar. Coast. Shelf Sci. 45 (2), 165–176.

Baskaran, M., Miller, C.J., Kumar, A., Andersen, E., Hui, J., Selegean, J.P., Barkach, J., 2015. Sediment accumulation rates and sediment dynamics using five different methods in a well-constrained impoundment: case study from Union Lake, Michigan. J. Great Lakes Res. 41 (2), 607–617.

Beasley, T.M., Jennings, C.D., 1984. Inventories of $^{239,\ 240}$Pu, ^{241}Am, ^{137}Cs, and ^{60}Co in Columbia River sediments from Hanford to the Columbia River estuary. Environmental Science & Technology 18 (3), 207–212.

Bowen, V.T., Noshkin, V.E., Livingston, H.D., Volchok, H.L., 1980. Fallout radionuclides in the Pacific Ocean: vertical and horizontal distributions, largely from GEOSECS stations. Earth Planet. Sci. Lett. 49 (2), 411–434.

Buesseler, K., Dai, M., Aoyama, M., Benitez-Nelson, C., Charmasson, S., Higley, K., Smith, J.N., 2017. Fukushima Daiichi–derived radionuclides in the ocean: transport, fate, and impacts. Annu. Rev. Mar. Sci. 9, 173–203.

Cao, H., Yang, H., Tang, X., Zhao, Q., Zhu, Z., Pu, L., 2001. Primary estimate on soil loss amounts in Yangtse Delta region using ^{137}Cs technique. J. Soil Water Conserv. 15 (1), 13–15 (in Chinese with English abstract).

Carpenter, R., Beasley, T.M., Zahnle, D., Somayajulu, B.L.K., 1987. Cycling of fallout (Pu, ^{241}Am, ^{137}Cs) and natural (U, Th, ^{210}Pb) radionuclides in Washington continental slope sediments. Geochim. Cosmochim. Acta 51 (7), 1897–1921.

Chen, C.T.A., 2009. Chemical and physical fronts in the Bohai, Yellow and East China seas. J. Mar. Syst. 78 (3), 394–410.

Chen, Z., Saito, Y., Kanai, Y., Wei, T., Li, L., Yao, H., Wang, Z., 2004. Low concentration of heavy metals in the Yangtze estuarine sediments, China: a diluting setting. Estuar. Coast. Shelf Sci. 60 (1), 91–100.

China Water Resources Committee (CWRC), 2014. Ministry of Water Resources of China (Ed.). China River Sediment BulletinChina Water Power Press, Beijing (in Chinese).

Chung, Y., Chang, W.C., 1995. Pb-210 fluxes and sedimentation rates on the lower continental slope between Taiwan and the South Okinawa Trough. Cont. Shelf Res. 15 (2–3), 149–164.

Cochran, J.K., Livingston, H.D., Hirschberg, D.J., Surprenant, L.D., 1987. Natural and anthropogenic radionuclide distributions in the northwest Atlantic Ocean. Earth Planet. Sci. Lett. 84 (2-3), 135–152.

Dai, Z., Du, J., Li, J., Li, W., Chen, J., 2008. Runoff characteristics of the Changjiang River during 2006: effect of extreme drought and the impounding of the Three Gorges Dam. Geophys. Res. Lett. 35 (7). https://doi.org/10.1029/2008GL033456.

DeMaster, D.J., McKee, B.A., Nittrouer, C.A., Jiangchu, Q., Guodong, C., 1985. Rates of sediment accumulation and particle reworking based on radiochemical measurements from continental shelf deposits in the East China Sea. Cont. Shelf Res. 4 (1–2), 143–158.

Deng, B., Zhang, J., Wu, Y., 2006. Recent sediment accumulation and carbon burial in the East China Sea. Glob. Biogeochem. Cycles 20 (3) (doi:10.1029/2005GB002559).

Dominik, J., Burrus, D., Vernet, J.P., 1987. Transport of the environmental radionuclides in an alpine watershed. Earth Planet. Sci. Lett. 84 (2–3), 165–180.

Dong, A., Zhai, S., Matthias, Z., Yu, Z., Chu, Z., 2009. Geochemistry characters of the core sediments in the Yangtze estuary and the response to human activities. Mar. Geol. Quat. Geol. 29 (4), 107–114 (in Chinese with English abstract).

Du, J., Wu, Y., Huang, D., Zhang, J., 2010. Use of ^{7}Be, ^{210}Pb and ^{137}Cs tracers to the transport of surface sediments of the Changjiang Estuary, China. J. Mar. Syst. 82 (4), 286–294.

Duan, L., Song, J., Yuan, H., Li, X., Li, N., 2013. Spatio-temporal distribution and environmental risk of arsenic in sediments of the East China Sea. Chem. Geol. 340, 21–31.

Duran, E.B., Povinec, P.P., Fowler, S.W., Airey, P.L., Hong, G.H., 2004. ^{137}Cs and $^{239+\ 240}$Pu levels in the Asia-Pacific regional seas. J. Environ. Radioact. 76 (1–2), 139–160.

Fan, D., Yang, Z., Mao, D., Guo, Z., 2001. Clay minerals and geochemistry of the sediments from the Yangtze and Yellow rivers. Mar. Geol. Quat. Geol. 21 (4), 7–12 (in Chinese with English abstract).

Fang, H., Yang, X., Zhang, X., Liang, A., 2006. Using ^{137}Cs tracer technique to evaluate erosion and deposition of black soil in Northeast China. Pedosphere 16 (2), 201–209.

Fang, T.H., Chen, J.L., Huh, C.A., 2007. Sedimentary phosphorus species and sedimentation flux in the East China Sea. Cont. Shelf Res. 27 (10−11), 1465–1476.

Feng, X., Jin, X., Zhang, W., Yu, X., Li, H., 2009. Variation of elements in sediments from the hypoxia zone of the Yangtze estuary and its response to sedimentary environment over the last 100 years. Mar. Geol. Quat. Geol. 29 (2), 25–32 (in Chinese with English abstract).

Fuller, C.C., van Geen, A., Baskaran, M., Anima, R., 1999. Sediment chronology in San Francisco Bay, California, defined by ^{210}Pb, ^{234}Th, ^{137}Cs, and ^{239,240}Pu. Mar. Chem. 64 (1–2), 7–27.

Gao, S., Wang, Y.P., Gao, J.H., 2011. Sediment retention at the Changjiang sub-aqueous delta over a 57-year period, in response to catchment changes. Estuar. Coast. Shelf Sci. 95 (1), 29–38.

Guan, B.X., 1994. Patterns and structures of the currents in Bohai, Huanghai and East China Seas. Oceanology of China Seas. Springer, Dordrecht, pp. 17–26.

Guo, Z., Lin, T., Zhang, G., Zheng, M., Zhang, Z., Hao, Y., Fang, M., 2007. The sedimentary fluxes of polycyclic aromatic hydrocarbons in the Yangtze River Estuary coastal sea for the past century. Sci. Total Environ. 386 (1–3), 33–41.

Hirose, K., Aoyama, M., 2003. Analysis of ^{137}Cs and ^{239,240}Pu concentrations in surface waters of the Pacific Ocean. Deep-Sea Res. II Top. Stud. Oceanogr. 50 (17–21), 2675–2700.

Hirose, K., Igarashi, Y., Aoyama, M., 2008. Analysis of the 50-year records of the atmospheric deposition of long-lived radionuclides in Japan. Appl. Radiat. Isot. 66 (11), 1675–1678.

Hong, G.H., Chung, C.S., Lee, S.H., Kim, S.H., Baskaran, M., Lee, H.M., ... Yang, D.B., 2006. Artificial radionuclides in the Yellow Sea: inputs and redistribution. Radioactivity in the Environment 8, 96–133.

Hu, Y., Liu, J., Zhuang, D., Cao, H., Yan, H., Yang, F., 2005. Distribution characteristics of ^{137}Cs in wind-eroded soil profile and its use in estimating wind erosion modulus. Chin. Sci. Bull. 50 (11), 1155–1159.

Hu, B., Li, G., Li, J., Yang, M., Wang, L., Bu, R., 2011a. Spatial variability of the ^{210}Pb sedimentation rates in the Bohai and Huanghai Seas and its influencing factors. Acta Sedimentol. Sin. 33 (6), 125–133 (in Chinese with English abstract).

Hu, L., Lin, T., Shi, X., Yang, Z., Wang, H., Zhang, G., Guo, Z., 2011b. The role of shelf mud depositional process and large river inputs on the fate of organochlorine pesticides in sediments of the Yellow and East China seas. Geophys. Res. Lett. 38 (3). https://doi.org/10.1029/2010GL045723.

Hu, D., Wu, L., Cai, W., Gupta, A.S., Ganachaud, A., Qiu, B., Wang, G., 2015. Pacific western boundary currents and their roles in climate. Nature 522 (7556), 299–308.

Hu, L., Shi, X., Bai, Y., Qiao, S., Li, L., Yu, Y., Guo, Z., 2016. Recent organic carbon sequestration in the shelf sediments of the Bohai Sea and Yellow Sea, China. J. Mar. Syst. 155, 50–58.

Hua, L., Zhang, Z., Feng, Y., Zhao, H., Li, J., Wang, X., 2006. Soil erosion and losses of nitrogen and phosphorus by using 137Cs tracer in the areas around Miyun reservoir. Transactions of the Chinese Society of Agricultural Engineering 22 (1), 73–78 (in Chinese with English abstract).

Huang, D., Fan, X., Xu, D., Tong, Y., Su, J., 2005. Westward shift of the Yellow Sea warm salty tongue. Geophys. Res. Lett. 32 (24). https://doi.org/10.1029/2005GL024749.

Huh, C.A., Chen, H.Y., 1999. History of lead pollution recorded in East China Sea sediments. Mar. Pollut. Bull. 38 (7), 545–549.

Huh, C.A., Su, C.C., 1999. Sedimentation dynamics in the East China Sea elucidated from ^{210}Pb, ^{137}Cs and ^{239,240}Pu. Mar. Geol. 160 (1–2), 183–196.

Hur, H.B., Jacobs, G.A., Teague, W.J., 1999. Monthly variations of water masses in the Yellow and East China Seas, November 6, 1998. J. Oceanogr. 55 (2), 171–184.

Iseki, K., Okamura, K., Kiyomoto, Y., 2003. Seasonality and composition of downward particulate fluxes at the continental shelf and Okinawa Trough in the East China Sea. Deep-Sea Res. II Top. Stud. Oceanogr. 50 (2), 457–473.

Ito, T., Aramaki, T., Kitamura, T., Otosaka, S., Suzuki, T., Togawa, O., Lishavskaya, T.S., 2003. Anthropogenic radionuclides in the Japan Sea: their distributions and transport processes. J. Environ. Radioact. 68 (3), 249–267.

Jia, Y.H., Wang, Z.Y., Zheng, X.M., Han, L.J., 2012. Estimation of soil erosion in the Xihanshui River Basin by using ^{137}Cs technique. International Journal of Sediment Research 27 (4), 486–497.

Jiang, H., 2010. Study on soil erosion in the farming—pastoral transitional zone of Northern China based on ^{137}Cs technology. Master Thesis. Inner Mongolia Normal University, Huhehot (in Chinese with English abstract).

Jin, P., Pu, L., Wang, J., Wang, Y., Pan, S., 2004. Preliminary study on using ^{137}Cs tracer method to estimate soil erosion of typical area: a case study on Xitiaoxi drainage area at upstream of Taihu Lake basin. Journal of Natural Resources 19 (1), 47–55 (in Chinese with English abstract).

Kagimoto, T., Yamagata, T., 1997. Seasonal transport variations of the Kuroshio: An OGCM simulation. J. Phys. Oceanogr. 27 (3), 403–418.

Kasamatsu, F., Inatomi, N., 1998. Effective environmental half-lives of ^{90}Sr and ^{137}Cs in the coastal seawater of Japan. Journal of Geophysical Research: Oceans 103 (C1), 1209–1217.

Kim, C.K., Kim, C.S., Yun, J.Y., Kim, K.H., 1997. Distribution of ^{3}H, ^{137}Cs and ^{239,240}Pu in the surface seawater around Korea. J. Radioanal. Nucl. Chem. 218 (1), 33.

Lee, H.J., Chough, S.K., 1989. Sediment distribution, dispersal and budget in the Yellow Sea. Mar. Geol. 87 (2–4), 195–205.

Lee, M., Lee, C., Hong, K., Choi, Y., Boo, B., 1996. Depth distribution of $^{239,\ 240}$Pu and ^{137}Cs in soils of South Korea. J. Radioanal. Nucl. Chem. 204 (1), 135–144.

Li, Q., Zhang, Y., Wang, H., 1993. A study on ^{137}Cs method used in determining soil erosion of small watershed. Journal of Yangtze River Scientific Research Institute 10 (4), 56–63 (in Chinese with English abstract).

Li, Q., Jiang, S., Sun, H., 1995. Determination of surface erosion of the small watersheds in the hilly area of purples soils in the upper reaches of the Yangtze River. Journal of Yangtze River Scientific Research Institute 12 (1), 51–56 (in Chinese with English abstract).

Li, F., Gao, S., Jia, J., Zhao, Y., 2002. Contemporary deposition rates of fine-grained sediment in the Bohai and Yellow Seas. Oceanologia et Limnologia Sinica 33 (4), 364–369.

Li, F., Li, X., Song, J., Wang, G., Cheng, P., Gao, S., 2006. Sediment flux and source in northern Yellow Sea by ^{210}Pb technique. Chin. J. Oceanol. Limnol. 24 (3), 255–263.

Li, M., Li, Z., Yao, W., Liu, P., 2009a. Estimating the erosion and deposition rates in a small watershed by the ^{137}Cs tracing method. Appl. Radiat. Isot. 67 (2), 362–366.

Li, H., Zhang, X., Wen, A., Shi, Z., 2009b. Erosion rate of purple soil on a cultivated slope in the Three Gorges Reservoir region using ^{137}Cs technique. Bulletin of Soil & Water Conservation 29 (5), 1–6 (in Chinese with English abstract).

Li, X., Bianchi, T.S., Allison, M.A., Chapman, P., Yang, G., 2013. Historical reconstruction of organic carbon decay and preservation in sediments on the East China Sea shelf. Journal of Geophysical Research: Biogeosciences 118 (3), 1079–1093.

Li, Y., Chappell, A., Nyamdavaa, B., Yu, H., Davaasuren, D., Zoljargal, K., 2015. Cost-effective sampling of ^{137}Cs-derived net soil redistribution: part 1–estimating the spatial mean across scales of variation. J. Environ. Radioact. 141, 97–105.

Li, Z., Liu, C., Dong, Y., Chang, X., Nie, X., Liu, L., Zeng, G., 2017. Response of soil organic carbon and nitrogen stocks to soil erosion and land use types in the Loess hilly–gully region of China. Soil Tillage Res. 166, 1–9.

Lian, E., Yang, S., Wu, H., Yang, C., Li, C., Liu, J.T., 2016. Kuroshio subsurface water feeds the wintertime Taiwan warm current on the inner East China Sea shelf. Journal of Geophysical Research: Oceans 121 (7), 4790–4803.

Liang, J., Dai, Q., Zhang, X., Gao, H., Liu, W., 2014. Study on soil erosion features of small catchment of karst plateau wetland by ^{137}Cs tracing technology. Journal of Nuclear Agricultural Sciences 28 (1), 116–122 (in Chinese with English abstract).

Lim, D.I., Choi, J.Y., Jung, H.S., Rho, K.C., Ahn, K.S., 2007. Recent sediment accumulation and origin of shelf mud deposits in the Yellow and East China Seas. Prog. Oceanogr. 73 (2), 145–159.

Lin, S., Huang, K.M., Chen, S.K., 2000. Organic carbon deposition and its control on iron sulfide formation of the southern East China Sea continental shelf sediments. Cont. Shelf Res. 20 (4–5), 619–635.

Lin, S., Hsieh, I.J., Huang, K.M., Wang, C.H., 2002. Influence of the Yangtze River and grain size on the spatial variations of heavy metals and organic carbon in the East China Sea continental shelf sediments. Chem. Geol. 182 (2–4), 377–394.

Lin, X., Yang, J., Guo, J., Zhang, Z., Yin, Y., Song, X., Zhang, X., 2011. An asymmetric upwind flow, Yellow Sea Warm Current: 1. New observations in the western Yellow Sea. Journal of Geophysical Research: Oceans 116 (C4). https://doi.org/10.1029/2010JC006513.

Lin, J., Zhu, Q., Hong, Y., Yuan, L., Liu, J., Xu, X., Wang, J., 2018. Synchronous response of sedimentary organic carbon accumulation on the inner shelf of the East China Sea to the water impoundment of Three Gorges and Gezhouba Dams. Journal of Oceanology and Limnology 36 (1), 153–164.

Liu, M., Fan, D., 2011. Geochemical records in the subaqueous Yangtze River delta and their responses to human activities in the past 60 years. Chin. Sci. Bull. 56 (6), 552–561.

Liu, K.K., Gong, G.C., Shyu, C.Z., Pai, S.C., Wei, C.L., Chao, S.Y., 1992. Response of Kuroshio upwelling to the onset of the northeast monsoon in the sea north of Taiwan: observations and a numerical simulation. Journal of Geophysical Research: Oceans 97 (C8), 12511–12526.

Liu, S.X., Shen, X., Wang, Y., Han, S., 1993. Preliminary analysis of the average monthly distribution and variation of the water masses in the Bohai, Yellow and East Sea. Acta Oceanol. Sin. 15 (4), 1–11 (in Chinese).

Liu, K.K., Tang, T.Y., Gong, G.C., Chen, L.Y., Shiah, F.K., 2000. Cross-shelf and along-shelf nutrient fluxes derived from flow fields and chemical hydrography observed in the southern East China Sea off northern Taiwan. Cont. Shelf Res. 20 (4–5), 493–523.

Liu, J., Zhu, R., Li, G., 2003. Rock magnetic properties of the fine-grained sediment on the outer shelf of the East China Sea: implication for provenance. Mar. Geol. 193 (3–4), 195–206.

Liu, J.P., Li, A.C., Xu, K.H., Velozzi, D.M., Yang, Z.S., Milliman, J.D., DeMaster, D.J., 2006. Sedimentary features of the Yangtze River-derived along-shelf clinoform deposit in the East China Sea. Cont. Shelf Res. 26 (17–18), 2141–2156.

Liu, S.F., Shi, X., Liu, Y., Zhu, A., Yang, G., 2009. Sedimentation rate of mud area in the East China Sea inner continental shelf. Mar. Geol. Quat. Geol. 29 (6), 5–11 (in Chinese with English abstract).

Liu, Z., Zheng, J., Pan, S., Dong, W., Yamada, M., Aono, T., Guo, Q., 2011. Pu and ^{137}Cs in the Yangtze River Estuary sediments: distribution and source identification. Environmental Science & Technology 45 (5), 1805–1811.

Liu, M., Zhang, A., Liao, Y., Chen, B., Fan, D., 2015. The environment quality of heavy metals in sediments from the central Bohai Sea. Mar. Pollut. Bull. 100 (1), 534–543.

Lu, X.X., Higgitt, D.L., 2000. Estimating erosion rates on sloping agricultural land in the Yangtze Three Gorges, China, from caesium-137 measurements. Catena 39 (1), 33–51.

Ma, J., Qiao, F., Xia, C., Kim, C.S., 2006. Effects of the Yellow Sea Warm Current on the winter temperature distribution in a numerical model. Journal of Geophysical Research: Oceans 111 (C11). https://doi.org/10.1029/2005JC003171.

Ma, W., Li, Z., Ding, K., Huang, B., Nie, X., Lu, Y., Xiao, H., 2016. Soil erosion, organic carbon and nitrogen dynamics in planted forests: a case study in a hilly catchment of Hunan Province, China. Soil Tillage Res. 155, 69–77.

Maderich, V., Bezhenar, R., Heling, R., de With, G., Jung, K. T., Myoung, J. G., … & Robertson, L. (2014). Regional long-term model of radioactivity dispersion and fate in the Northwestern Pacific and adjacent seas: application to the Fukushima Dai-ichi accident. J. Environ. Radioact., 131, 4–18.

McKee, B.A., Nittrouer, C.A., DeMaster, D.J., 1983. Concepts of sediment deposition and accumulation applied to the continental shelf near the mouth of the Yangtze River. Geology 11 (11), 631–633.

Menzel, R.G., Jung, P.K., Ryu, K.S., Um, K.T., 1987. Estimating soil erosion losses in Korea with fallout cesium-137. International Journal of Radiation Applications and Instrumentation. Part A. Applied Radiation and Isotopes 38 (6), 451–454.

Meusburger, K., Mabit, L., Park, J.H., Sandor, T., Alewell, C., 2013. Combined use of stable isotopes and fallout radionuclides as soil erosion indicators in a forested mountain site, South Korea. Biogeosciences 10. https://doi.org/10.5194/bg-10-5627-2013.

Milliman, J.D., Farnsworth, K.L., 2013. River Discharge to the Coastal Ocean: A Global Synthesis. Cambridge University Press, Cambridge.

Milliman, J.D., Huang-Ting, S., Zuo-Sheng, Y., Mead, R.H., 1985. Transport and deposition of river sediment in the Changjiang estuary and adjacent continental shelf. Cont. Shelf Res. 4 (1–2), 37–45.

Nagaya, Y., Nakamura, K., 1992. ^{239,240}Pu and ^{137}Cs in the east China and the Yellow seas. J. Oceanogr. 48 (1), 23–35.

Oguri, K., Matsumoto, E., Yamada, M., Saito, Y., Iseki, K., 2003. Sediment accumulation rates and budgets of depositing particles of the East China Sea. Deep-Sea Res. II Top. Stud. Oceanogr. 50 (2), 513–528.

Ohnuki, T., Kozai, N., 2013. Adsorption behavior of radioactive cesium by non-mica minerals. J. Nucl. Sci. Technol. 50 (4), 369–375.

Pfitzner, J., Brunskill, G., Zagorskis, I., 2004. ^{137}Cs and excess ^{210}Pb deposition patterns in estuarine and marine sediment in the central region of the Great Barrier Reef Lagoon, north-eastern Australia. J. Environ. Radioact. 76 (1–2), 81–102.

Povinec, P.P., Livingston, H.D., Shima, S., Aoyama, M., Gastaud, J., Goroncy, I., La Rosa, J., 2003. IAEA'97 expedition to the NW Pacific Ocean—results of oceanographic and radionuclide investigations of the water column. Deep-Sea Res. II Top. Stud. Oceanogr. 50 (17–21), 2607–2637.

Povinec, P.P., Hirose, K., Honda, T., Ito, T., Scott, E.M., Togawa, O., 2004. Spatial distribution of ^{3}H, ^{90}Sr, ^{137}Cs and ^{239,240}Pu in surface waters of the Pacific and Indian Oceans—GLOMARD database. J. Environ. Radioact. 76 (1–2), 113–137.

Povinec, P.P., Aoyama, M., Fukasawa, M., Hirose, K., Komura, K., Sanchez-Cabeza, J.A., Sýkora, I., 2011. ^{137}Cs water profiles in the South Indian Ocean—an evidence for accumulation of pollutants in the subtropical gyre. Prog. Oceanogr. 89 (1–4), 17–30.

Pu, L., Zhao, Y., Jin, P., Wang, J., Huang, X., 2004. Application of ^{137}Cs as tracing method to study soil erosion on sloping lands in the hilly red soil area: a case study in Fengcheng city, Jiangxi province. Resources & Environment in the Yangtze Basin 13 (6), 562–567 (in Chinese with English abstract).

Qi, J., Yin, B., Zhang, Q., Yang, D., Xu, Z., 2014. Analysis of seasonal variation of water masses in East China Sea. Chin. J. Oceanol. Limnol. 32 (4), 958–971.

Qiao, S., Shi, X., Wang, G., Zhou, L., Hu, B., Hu, L., Liu, S., 2017. Sediment accumulation and budget in the Bohai Sea, Yellow Sea and East China Sea. Mar. Geol. 390, 270–281.

Qin, Y., Zhao, Y., Chen, L., Zhao, S., 1996. Geology of the East China Sea. Science Press, Beijing.

Quine, T.A., Walling, D.E., Zhang, X., Wang, Y., 1992. Investigation of Soil Erosion on Terraced Fields near Yanting, Sichuan Province, China, Using Caesium-137. vol. 209. International Association of Hydrological Sciences Publication, pp. 155–168.

Ravichandran, M., Baskaran, M., Santschi, P.H., Bianchi, T.S., 1995. Geochronology of sediments in the Sabine-Neches estuary, Texas, USA. Chem. Geol. 125 (3–4), 291–306.

Shao, Q., Xiao, T., Liu, J., Qi, Y., 2011. Soil erosion rates and characteristics of typical alpine meadow using ^{137}Cs technique in Qinghai-Tibet Plateau. Chin. Sci. Bull. 56 (16), 1708–1713.

Smith, J.N., Ellis, K.M., 1982. Transport mechanism for Pb-210, Cs-137 and Pu fallout radionuclides through fluvial-marine systems. Geochim. Cosmochim. Acta 46 (6), 941–954.

Su, J.L., 2001. A review of circulation dynamics of the coastal oceans near China. Acta Oceanol. Sin. 23 (4), 1–16 (In Chinese with English abstract).

Su, C.C., Huh, C.A., 2002. ^{210}Pb, ^{137}Cs and ^{239,240}Pu in East China Sea sediments: sources, pathways and budgets of sediments and radionuclides. Mar. Geol. 183 (1–4), 163–178.

Su, Z., Li, Y., Zhang, J., Xiong, D., Dong, Y., Zhang, S., Yang, D., 2017. Spatial variation in soil, SOC, and total N redistribution on affected and non-affected slope terraces due to the 8.0 Wenchuan Earthquake in 2008 by using ^{137}Cs technique. Catena 155, 191–199.

Takata, H., Hasegawa, K., Oikawa, S., Kudo, N., Ikenoue, T., Isono, R.S., Kusakabe, M., 2015. Remobilization of radiocesium on riverine particles in seawater: the contribution of desorption to the export flux to the marine environment. Mar. Chem. 176, 51–63.

Tang, X., Yang, H., Du, M., Zhao, Q., Li, R., 2006. Identification of ^{137}Cs reference sites in southeastern China. Pedosphere 16 (4), 468–476.

Tsubono, T., Misumi, K., Tsumune, D., Bryan, F.O., Hirose, K., Aoyama, M., 2016. Evaluation of radioactive cesium impact from atmospheric deposition and direct release fluxes into the North Pacific from the Fukushima Daiichi nuclear power plant. Deep-Sea Res. I Oceanogr. Res. Pap. 115, 10–21.

Wang, Q., Yang, S., 2013. Clay mineralogy indicates the Holocene monsoon climate in the Changjiang (Yangtze River) catchment, China. Appl. Clay Sci. 74, 28–36.

Wang, Y., Fu, B., Lu, Y., Chen, L., 2011. Effects of vegetation restoration on soil organic carbon sequestration at multiple scales in semi-arid Loess Plateau, China. Catena 85 (1), 58–66.

Wang, Y., Niu, F., Wu, Q., Gao, Z., 2014. Assessing soil erosion and control factors by radiometric technique in the source region of the Yellow River, Tibetan Plateau. Quat. Res. 81 (3), 538–544.

Wang, J., Du, J., Baskaran, M., Zhang, J., 2016. Mobile mud dynamics in the East China Sea elucidated using ^{210}Pb, ^{137}Cs, ^{7}Be, and ^{234}Th as tracers. Journal of Geophysical Research: Oceans 121 (1), 224–239.

Wang, J., Baskaran, M., Hou, X., Du, J., Zhang, J., 2017a. Historical changes in ^{239}Pu and ^{240}Pu sources in sedimentary records in the East China Sea: implications for provenance and transportation. Earth Planet. Sci. Lett. 466, 32–42.

Wang, J., Baskaran, M., Niedermiller, J., 2017b. Mobility of ^{137}Cs in freshwater lakes: a mass balance and diffusion study of Lake St. Clair, Southeast Michigan, USA. Geochim. Cosmochim. Acta 218, 323–342.

Wang, J., Fan, Y., Liu, D., Lu, T., Hou, X., Du, J., 2018a. Spatial and vertical distribution of ^{129}I and ^{127}I in the East China Sea: inventory, source and transportation. Sci. Total Environ. 652, 177–188.

Wang, J., Zhang, W., Baskaran, M., Du, J., Zhou, F., Wu, H., 2018b. Fingerprinting sediment transport in river-dominated margins using combined mineral magnetic and radionuclide methods. J. Geophys. Res. Oceans 123, 5360–5374.

Wang, X., Baskaran, M., Su, K., Du, J., 2018c. The important role of submarine groundwater discharge (SGD) to derive nutrient fluxes into river dominated ocean margins—the East China Sea. Mar. Chem. 204, 121–132.

Wen, C., 2012. Researches on the Post-Glacial Sedimentary Evolutions of the Three Typical Depositions on the Western South Yellow Sea. (PhD thesis). Ocean University of China, Qingdao (in Chinese with English abstract).

Wong, G.T., Chao, S.Y., Li, Y.H., Shiah, F.K., 2000. The Kuroshio edge exchange processes (KEEP) study—an introduction to hypotheses and highlights. Cont. Shelf Res. 20 (4–5), 335–347.

Wu, J., 2018. Impacts of Fukushima Daiichi Nuclear Power Plant accident on the Western North Pacific and the China Seas: evaluation based on field observation of ^{137}Cs. Mar. Pollut. Bull. 127, 45–53.
Wu, H., Zhu, J., Shen, J., Wang, H., 2011. Tidal modulation on the Changjiang River plume in summer. Journal of Geophysical Research: Oceans 116 (C8). https://doi.org/10.1029/2011JC007209.
Wu, J., Zhou, K., Dai, M., 2013. Impacts of the Fukushima nuclear accident on the China seas: evaluation based on anthropogenic radionuclide ^{137}Cs. Chin. Sci. Bull. 58 (4–5), 552–558.
Wu, H., Shen, J., Zhu, J., Zhang, J., Li, L., 2014. Characteristics of the Changjiang plume and its extension along the Jiangsu Coast. Cont. Shelf Res. 76, 108–123.
Xia, X., Xie, Q., Li, Y., Li, B., Feng, Y., 1999. ^{137}Cs and ^{210}Pb profiles of the seabed cores along the East China Sea coast and their implications to sedimentary environment. Donghai Marine Science 17 (1), 20–27 (in Chinese with English abstract).
Xia, X., Yang, H., Li, Y., Li, B., Pan, S., 2004. Modern sedimentation rates in the contiguous sea area of Changjiang Estuary and Huangzhou Bay. Acta Sedimentol. Sin. 22 (1), 130–134 (in Chinese with English abstract).
Xie, Q., Li, B., Xia, X., Li, Y., Van Weering, T.C.E., Berger, G.W., 1994. Spatial and temporal variations of tidal flat in the Oujiang Estuary in China. Acta Geograph. Sin. 49 (6), 509–516 (in Chinese with English abstract).
Xie, S.P., Hafner, J., Tanimoto, Y., Liu, W.T., Tokinaga, H., Xu, H., 2002. Bathymetric effect on the winter sea surface temperature and climate of the Yellow and East China Seas. Geophys. Res. Lett. 29 (24). https://doi.org/10.1029/2002GL015884.
Xu, Y., Qiao, J., Pan, S., Hou, X., Roos, P., Cao, L., 2015. Plutonium as a tracer for soil erosion assessment in northeast China. Sci. Total Environ. 511, 176–185.
Xu, X., Hong, Y., Zhou, Q., Liu, J., Yuan, L., Wang, J., 2018. Century-scale high-resolution black carbon records in sediment cores from the South Yellow Sea, China. Journal of Oceanology and Limnology 36 (1), 114–127.
Yamada, M., Zheng, J., Wang, Z.L., 2006. ^{137}Cs, $^{239+240}$Pu and ^{240}Pu/^{239}Pu atom ratios in the surface waters of the western North Pacific Ocean, eastern Indian Ocean and their adjacent seas. Sci. Total Environ. 366 (1), 242–252.
Yan, P., Shi, P., 2004. Using the ^{137}Cs technique to estimate wind erosion in Gonghe Basin, Qinghai Province, China. Soil Sci. 169 (4), 295–305.
Yan, B., Yang, J., 2005. Study on black soil erosion rate and the transformation of soil quality influenced by erosion. Geogr. Res. 23 (1), 22–29 (in Chinese with English abstract).
Yan, D., Wen, A., Bao, Y., Zhang, 2008. The distribution of ^{137}Cs in hilly upland soil the Qianzhong Karst Plateau. Earth & Environment 36 (4), 342–347 (in Chinese with English abstract).
Yanagi, T., Takahashi, S., Hoshika, A., Tanimoto, T., 1996. Seasonal variation in the transport of suspended matter in the East China Sea. J. Oceanogr. 52 (5), 539–552.
Yanagi, T., Shimizu, T., Lie, H.J., 1998. Detailed structure of the Kuroshio frontal eddy along the shelf edge of the East China Sea. Cont. Shelf Res. 18 (9), 1039–1056.
Yang, Z., Chen, X., 2007. Centurial high resolution records of sediment grain-size variation in the mud area off the Changjiang (Yangtze river) estuary and its influencial factors. Quaternary Sciences 27 (5), 690–699 (in Chinese with English abstract).
Yang, S.Y., Youn, J.S., 2007. Geochemical compositions and provenance discrimination of the central south Yellow Sea sediments. Mar. Geol. 243 (1–4), 229–241.
Yang, S.L., Liu, G., Du, R., Zhang, B., 1993. Study on the modern sedimentation rate through ^{210}Pb age dating in Liaodong Bay. Acta Sedimentol. Sin. 11 (1), 128–135 (in Chinese with English abstract).
Yang, Y., Yan, B., Zhu, H., 2011. Estimating soil erosion in Northeast China using ^{137}Cs and $^{210}Pb_{ex}$. Pedosphere 21 (6), 706–711.
Yang, D., Yin, B., Liu, Z., Bai, T., Qi, J., Chen, H., 2012. Numerical study on the pattern and origins of Kuroshio branches in the bottom water of southern East China Sea in summer. Journal of Geophysical Research: Oceans 117 (C2). https://doi.org/10.1029/2011JC007528.
Youn, J., Kim, T.J., 2011. Geochemical composition and provenance of muddy shelf deposits in the East China Sea. Quat. Int. 230 (1), 3–12.
Zhang, X., Higgitt, D.L., Walling, D.E., 1990. A preliminary assessment of the potential for using caesium-137 to estimate rates of soil erosion in the Loess Plateau of China. Hydrol. Sci. J. 35 (3), 243–252.
Zhang, X., Quine, T.A., Walling, D.E., Li, Z., 1994. Application of the caesium-137 technique in a study of soil erosion on gully slopes in a yuan area of the Loess Plateau near Xifeng, Gansu Province, China. Geografiska Annaler: Series A, Physical Geography 76 (1–2), 103–120.
Zhang, X., Walling, D.E., Quine, T.A., Wen, A., 1997. Use of reservoir deposits and caesium-137 measurements to investigate the erosional response of a small drainage basin in the rolling Loess Plateau region of China. Land Degrad. Dev. 8 (1), 1–16.
Zhang, X., Quine, T.A., Walling, D.E., 1998. Soil erosion rates on sloping cultivated land on the Loess Plateau near Ansai, Shaanxi Province, China: an investigation using ^{137}Cs and rill measurements. Hydrol. Process. 12 (1), 171–189.
Zhang, C., Zou, X., Dong, G., Zhang, X., Qin, Z., 2002. Characteristics of ^{137}Cs deposition in steppe area. Chin. Sci. Bull. 47 (10), 848–853.
Zhang, X., Zhang, Y., Wen, A., Feng, M., 2003. Assessment of soil losses on cultivated land by using the ^{137}Cs technique in the Upper Yangtze River Basin of China. Soil Tillage Res. 69 (1–2), 99–106.
Zhang, Y., Peng, B.Z., Gao, X., Yang, H., 2004. Degradation of soil properties due to erosion on sloping land in southern Jiangsu Province, China. Pedosphere 14 (1), 17–26.
Zhang, Z., Li, S., Dong, Y., Wang, Q., Xiao, Lu, J., 2005. Deposition rate and geochemical characters of sediments in Zhejiang offshore. Mar. Geol. Quat. Geol. 25 (3), 15–24 (in Chinese with English abstract).
Zhang, X., Qi, Y., Walling, D.E., He, X., Wen, A., Fu, J., 2006. A preliminary assessment of the potential for using $^{210}Pb_{ex}$ measurement to estimate soil redistribution rates on cultivated slopes in the Sichuan Hilly Basin of China. Catena 68, 1–9.
Zhang, J., Liu, S.M., Ren, J.L., Wu, Y., Zhang, G.L., 2007. Nutrient gradients from the eutrophic Changjiang (Yangtze River) Estuary to the oligotrophic Kuroshio waters and re-evaluation of budgets for the East China Sea Shelf. Prog. Oceanogr. 74 (4), 449–478.
Zhang, R., Pan, S., Wang, Y., 2009a. Sedimentation rates and characteristics of radionuclide ^{210}Pb at the subaqueous delta in Changjiang Estuary. Acta Sedimentol. Sin. 27 (4), 704–713 (in Chinese with English abstract).
Zhang, M., Yang, H., Wang, X., Wang, Y., Xu, C., Yang, J., Rong, J., 2009b. Soil ^{137}Cs background values in monsoon region of China. Journal of Nuclear Agricultural Sciences 23 (4), 669–675 (in Chinese with English abstract).
Zhang, R.M., Zhang, G., Huang, B., Zhang, X., 2009c. Analysis of modern sedimentation rate in nearshore area of the Shandong Peninsula. Marine Geology Letters 25 (9), 15–18 (in Chinese with English abstract).
Zhang, L., Zhang, Y., Li, H., 2010. Soil erosion and pollutant loss of Danjiangkou city in south China based on ^{137}Cs technique. Mechanic Automation and Control Engineering (MACE), 2010 International Conference *on*. IEEE, pp. 1900–1903.
Zhang, C., Yang, S., Pan, X., Zhang, J., 2011. Estimation of farmland soil wind erosion using RTK GPS measurements and the ^{137}Cs technique: a case study in Kangbao County, Hebei province, northern China. Soil Tillage Res. 112 (2), 140–148.
Zhang, Y., Wen, A., Yan, D., Guo, J., Ju, Z., 2014. Using ^{137}Cs technique to study soil erosion in Chishui River region. Earth & Environment 42 (2), 187–192 (in Chinese with English abstract).
Zhang, H., Nie, X., Cheng, X., 2015. ^{137}Cs tracing of soil erosion and its impact on soil nutrients across subsidence slope induced by coal mining. Transactions of the Chinese Society of Agricultural Engineering 31 (4), 137–143 (in Chinese with English abstract).
Zhao, Y., Li, F., Demaster, D.J., Nittrouer, C.A., Milliman, J.D., 1991. Preliminary studies on sedimentation rate and sediment flux of the South Huanghai Sea. Oceanologia et Limnologia Sinica 22 (1), 37–43 (in Chinese with English abstract).
Zhao, Y., Yuan, J., Xu, C., Du, C., Chang, Y., 2005. Application of ^{137}Cs tracer technique to estimate the wind erosion rate of castanozem in Luanhe River source area. Acta Sci. Circumst. 254 (2), 562–566 (in Chinese with English abstract).
Zhao, L., Liu, D., Wang, J., Du, J., Hou, X., Jiang, Y., 2018. Spatial and vertical distribution of radiocesium in seawater of the East China Sea. Mar. Pollut. Bull. 128, 361–368.
Zheng, J., He, X., Walling, D.E., Zhang, X.B., Flanagan, D., Qi, Y.Q., 2007. Assessing soil erosion rates on manually-tilled hillslopes in the Sichuan Hilly Basin using ^{137}Cs and $^{210}Pb_{ex}$ measurements. Pedosphere 17 (3), 273–283.
Zhou, L., Liu, J., Saito, Y., Gao, M., Diao, S., Qiu, J., Pei, S., 2016. Modern sediment characteristics and accumulation rates from the delta front to prodelta of the Yellow River (Huanghe). Geo-Mar. Lett. 36 (4), 247–258.
Zhou, P., Li, D., Zhao, L., Li, H., Zhao, F., Zheng, Y., Cai, W., 2018. Radioactive status of seawater and its assessment in the northeast South China Sea and the Luzon Strait and its adjacent areas from 2011 to 2014. Mar. Pollut. Bull. 131, 163–173.
Zhu, H., Li, S., Wu, F., Sun, F., Liu, W., Yang, W., 1991. Radioactivity in the coastal waters of the Bohai and Yellow Seas of China. J. Environ. Radioact. 14 (3), 193–209.
Zhu, Z.Y., Wu, Y., Zhang, J., Du, J.Z., Zhang, G.S., 2014. Reconstruction of anthropogenic eutrophication in the region off the Changjiang Estuary and central Yellow Sea: from decades to centuries. Cont. Shelf Res. 72, 152–162.